Received 4 April 2023; revised 20 May 2023; accepted 11 June 2023. Date of publication 20 June 2023; date of current version 10 July 2023.

Digital Object Identifier 10.1109/OJCOMS.2023.3287986

Near-Optimal Nonbinary Index Assignment for Equiprobable Lattice Quantizers

YUNXIANG YAO (Student Member, IEEE), AND WAI HO MOW (Senior Member, IEEE)

Department of Electronic and Computer Engineering, The Hong Kong University of Science and Technology, Hong Kong

CORRESPONDING AUTHOR: Y. YAO (e-mail: yyaoaj@ust.hk)

This work was supported by the Hong Kong Research Grants Council under Project GRF 16214422.

Part of this work has been presented at the IEEE International Conference on Communications (ICC) in 2020 [1] [DOI: 10.1109/ICC40277.2020.9149320].

ABSTRACT Index assignment (IA) is a low-complexity joint source-channel coding technique that has the potential for use in low-latency and low-power applications, such as wireless sensor networks (WSNs). Though binary IA has been extensively studied for assigning binary indices to quantized codewords (or symbols) under the assumption of binary symmetric channels (BSCs), real-world scenarios often use M-ary modulations. Directly applying binary IAs designed for BSCs to M-ary modulations results in suboptimal performance. In this paper, we investigate the M-ary IA, which assigns M-ary labels to quantized codewords (or symbols), assuming the use of a equiprobable lattice quantizer. For such a system, we derive a tight performance bound and propose a near-optimal IA scheme based on a two-step design. In addition, we propose explicit IA constructions for practical modulation schemes, including PAM, QAM, and PSK. Our proposed IA design is rigorously proven to be optimal for 3-PSK and QPSK, whereas for larger modulation orders, the proposed IA constructions approach the bounds within small gaps. Our simulations show that the constructed IA scheme can achieve significant energy savings compared to the conventional binary IA scheme. Specifically, in some WSN scenarios, the proposed IA for 16-QAM is shown to achieve significant reductions in energy consumption relative to the conventional binary counterpart.

INDEX TERMS Discrete memoryless channel, index assignment, joint source-channel coding, quantization.

I. INTRODUCTION

THE DRAMATIC growth of wireless networks in recent decades has enabled the broad utilization of the Internet of Things (IoT) across numerous applications, including smart homes, smart cities, and beyond [2]. Wireless sensor networks (WSNs) play a critical role in IoT by collecting data from the environment and transmitting it to other sensor nodes [2], [3], [4], [5], [6]. However, energy consumption is a major challenge in WSNs, as sensor nodes are typically powered by batteries and deployed in remote locations where battery recharge is challenging or impossible [6], [7], [8]. It is important to reduce power consumption while maintaining reliable data transmission to extend the battery life of the sensor node. In many IoT applications, WSNs need to transmit the sensed information with low latency in the form of quantized data after being processed by a quantizer [6]. To achieve this, *joint source-channel coding* (JSCC) is an effective low-latency approach that reduces power consumption while maintaining transmission quality [9], [10], [11], [12]. This paper focuses on a low-complexity JSCC technique called *index assignment* (IA). IA is a technique that involves assigning zero-redundancy codes to label quantized codewords (or symbols) in a way that minimizes the distortion of quantized codewords caused by channel errors [13]. The design of the labeling rule can be done offline, enabling IA to be integrated into a communication system with low latency and low power consumption. Its low complexity and error-resistance properties make it a promising solution for energy-efficient applications, such as WSNs [9], [14], [15].

In conventional IA problems, binary indices are used to label quantized codewords or symbols, which are subsequently transmitted over a binary symmetric channel (BSC) [16]. Despite the extensive research into binary IA, finding the optimal binary IA for general quantizers and sources is still an open problem. The only known case of

optimal binary IA is for uniform quantizers with uniform sources, where the *natural binary code* (NBC) was known to minimize channel mean-squared distortion (MSD) [17], [18], [19], [20]. Later, Farber and Zeger proved the optimality of the NBC for quantizers with uniform encoders and channel-optimized decoders [21]. The problem of finding the optimal IA for general source models and quantizers is known to be NP-hard [22], and even finding the optimal IA for a quantizer with a small codebook is challenging due to its high complexity [13]. Although there are heuristics for designing good but not necessarily optimal IAs [23], [24], [25], [26], [27], [28], they still require a significant amount of time to yield good results.

In practical applications, M-ary modulations, such as M-PSK, M-PAM, and M-QAM, are often used to improve bandwidth efficiency. To apply binary IAs designed for BSC to M-ary transmission, a BSC can be modeled from the M-ary transmission by considering the bit error rate (BER) as the crossover probability [29]. Additionally, the binary Gray code is commonly utilized to modulate index bits as channel symbols in order to minimize the BER. However, even if the binary IA and modulation mapping are optimally designed individually, their combination is suboptimal for minimizing the MSD [30]. To address this problem, we propose an alternative design that uses an M-ary IA to label the quantized codewords (or symbols) of an M^L-point quantizer by M-ary channel symbols. To the best of our knowledge, there are few works related to this M-ary IA problem. Skoglund introduced a method for analyzing the channel MSD based on the diagonalization of the transition matrix for general quantizers and M-ary discrete memoryless channels (DMCs) [16]. Ben-David and Malah [31] and Wu et al. [32] studied performance bounds on the channel MSD. Chan and Mow investigated the IA that maps quantized symbols of an equiprobable M-level scalar quantizer directly to M-PSK symbols [33], which is a special case of our proposed M-ary IA with $L = 1$. The *zigzag mapping* was introduced and proven to be an optimal IA for this special case [33], [34]. However, the zigzag mapping is only applicable when the size of the quantizer and the size of the M-PSK constellation are the same. Finding optimal or near-optimal M-ary IA designs for $L > 1$ and other modulation schemes remains an open challenge.

Vector quantizers are widely used in various applications to improve data compression efficiency. However, designing and implementing unstructured vector quantizers have been shown to be highly complex [35], [36]. Hence, suboptimal structured quantizers, such as multistage vector quantizers, tree-structured quantizers, and lattice vector quantizers, have been proposed to simplify complexity, albeit with reduced performance [36], [37], [38]. Lattice vector quantizers have been demonstrated to be practical in many applications and have been well-studied theoretically. A particular case of lattice vector quantizers referred to as "binary lattice quantizers" has been studied by Mehes and Zeger [37]. These quantizers can also be considered as a special case of a multistage vector quantizer, where each stage contains only two codewords [37]. The binary lattice quantizers have been shown to be robust against the noise of binary channels, particularly under "channel-mismatch" conditions when the exact level of the channel noise is not perfectly known [37]. This robustness makes the quantizer practical. Additionally, the quantizer is compatible with IA schemes, which are also robust to changes in channel conditions [39]. Therefore, for M-ary transmissions, we introduce an M-ary generalized version of the binary lattice quantizers and investigate the M-ary IA design to achieve optimal or near-optimal performance.

In this work, we propose a design for an M-ary IA to label the quantized codewords (or symbols) of an M^L-point quantizer using M-ary channel symbols, with the objective of minimizing the channel MSD. We first derive a performance bound on channel MSD and, together with a novel M-ary generalization of NBC, devise a two-step design for the M-ary IA. In the first stage, we assign length-L index vectors consisting of M-ary index symbols to the quantized codewords (or symbols). In the second stage, we map these M-ary index symbols to M-ary modulated channel symbols. Our contributions are summarized below:

1) We derive a tight lower bound on channel MSD for equiprobable quantizers and general M-ary DMCs, including both symmetric and asymmetric channels. We also derive explicit forms of the bound for practical modulation schemes including PAM, QAM, and PSK.
2) We propose a novel M-ary IA structure called the *natural M-ary code* (NMC), which is generalized from the NBC. We derive its corresponding channel MSD. By defining a ratio to represent the gap between the lower bound and the channel MSD, the IA problem is transformed into a two-step design: first, label the quantized codewords by M-ary index vectors with NMC, and second, modulate the resulting M-ary index symbols as channel symbols to minimizing the gap.
3) We provide explicit near-optimal IAs based on the two-step design for specific modulation schemes including PAM, QAM, and PSK. We derive closed-form eigendecompositions for the DMC arising from these modulation transmissions and analyze the performances of the proposed IAs. Notably, the proposed IA for PSK is rigorously proven to be optimal for 3-PSK and QPSK.
4) We introduce an energy-efficient WSN model and demonstrate that our proposed M-ary IAs can achieve significant energy savings compared to conventional binary IA in the WSN application.

The remainder of the paper is organized as follows. Section II formulates the M-ary IA problem. In Section III, we derive a lower bound on channel MSD and propose an M-ary IA generalized from the NBC. We then propose a two-step framework for obtaining near-optimal IA schemes. In Section IV, we present explicit IA constructions for specific modulations and provide asymptotic analyses to demonstrate their near-optimality. We prove the optimality

of the proposed IA for M-PSK when $M = 3, 4$. In Section V, simulation results show that the proposed IAs have performances that are close to the performance bounds. Finally, we provide simulations for a WSN model to demonstrate the significant energy savings achieved by the proposed M-ary IA compared to the conventional binary IA scheme.

Notations: Scalars are represented by italic letters. Vectors and matrices are represented by bold-face lower-case and uppercase letters, respectively. The i-th element of vector $\mathbf{a}$ is denoted by a_i, and the (i, j)-th element of matrix $\mathbf{A}$ is denoted by $A(i, j)$. The all-1 column vector and the identity matrix are denoted by $\mathbf{1}$ and $\mathbf{I}$, respectively. The sets of real numbers and integers are denoted by $\mathbb{R}$ and $\mathbb{Z}$, respectively. The superscript $(\cdot)^\top$ denotes the transpose of a matrix or a vector. The Kronecker product is denoted by the binary operator $\otimes$. The trace of a matrix is denoted by $\mathrm{Tr}(\cdot)$.

II. PROBLEM FORMULATION

A. MEAN-SQUARED DISTORTION

In this paper, we consider a communication system that employs a k-dimensional vector quantizer for data compression. It is worth noting that a scalar quantizer is a special case of the vector quantizer when $k = 1$. The data source is modeled as a k-dimensional real-valued random vector $\boldsymbol{X} \in \mathbb{R}^k$, with its probability density function (PDF) $p_{\boldsymbol{X}}(\mathbf{x})$, where $\mathbf{x}$ denotes a realization of $\boldsymbol{X}$. The data source is compressed through a vector quantizer that is defined by a codebook of M^L quantized codewords, given by

$$\mathcal{Y} = \left\{\mathbf{y}_i \in \mathbb{R}^k | i = 0, 1, \ldots, M^L - 1\right\}. \tag{1}$$

The quantizer maps a data sample $\mathbf{x}$ to the codeword closest to it, as determined by the quantization function given by

$$\mathsf{F}_Q(\mathbf{x}) = \mathbf{y}_i, \quad d_E(\mathbf{x}, \mathbf{y}_i) < d_E\big(\mathbf{x}, \mathbf{y}_j\big), \ \forall j \neq i. \tag{2}$$

where $d_E(\mathbf{x}, \mathbf{y})$ denotes the Euclidean distance between two vectors $\mathbf{x}$ and $\mathbf{y}$. Based on the quantization function, the quantization cell is defined by

$$\mathcal{R}_i = \left\{\mathbf{x} \in \mathbb{R}^k | \mathsf{F}_Q(\mathbf{x}) = \mathbf{y}_i\right\}, \quad i = 0, 1, \ldots, M^L - 1, \tag{3}$$

with $\cup_{i=0}^{M^L-1} \mathcal{R}_i = \mathbb{R}^k$ and $\mathcal{R}_i \cap \mathcal{R}_j = \emptyset, \forall i \neq j$.

The performance of the system is evaluated using MSD, which is defined by

$$D = \sum_{i=0}^{M^L-1} \sum_{j=0}^{M^L-1} P\big(\mathbf{y}_j|\mathbf{y}_i\big) \int_{\mathcal{R}_i} \|\mathbf{x} - \mathbf{y}_j\|^2 p_{\boldsymbol{X}}(\mathbf{x}) d\mathbf{x}, \tag{4}$$

where $P(\mathbf{y}_j|\mathbf{y}_i)$ is the probability that $\mathbf{y}_j$ is reconstructed given that $\mathbf{y}_i$ is transmitted. The probability that $\mathbf{x}$ lies in the i-th quantization cell is denoted by $P_i = \int_{\mathcal{R}_i} p_{\boldsymbol{X}}(\mathbf{x}) d\mathbf{x}$, and the centroid of the i-th cell is represented by $\mathbf{c}_i = \frac{\int_{\mathcal{R}_i} \mathbf{x} p_{\boldsymbol{X}}(\mathbf{x}) d\mathbf{x}}{P_i}$. The MSD can be decomposed into two terms [40]: source MSD (D_Q) and channel MSD (D_C), given by

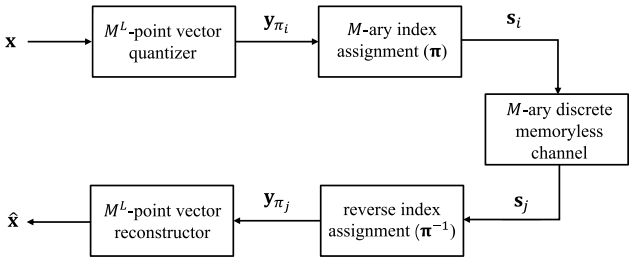

FIGURE 1. Block diagram of the communication system considered in this paper, featuring a vector quantizer with M^L codewords, an M-ary IA scheme, and an M-ary DMC.

$$\begin{aligned} D &= D_Q + D_C \\ &= \sum_{i=0}^{M^L-1} \int_{\mathcal{R}_i} \|\mathbf{x} - \mathbf{c}_i\|^2 p_{\boldsymbol{X}}(\mathbf{x}) d\mathbf{x} \\ &\quad + \sum_{i=0}^{M^L-1} \sum_{j=0}^{M^L-1} P_i P\big(\mathbf{y}_j|\mathbf{y}_i\big) \|\mathbf{c}_i - \mathbf{y}_j\|^2. \end{aligned} \tag{5}$$

Note that the source MSD depends solely on the quantizer and is not influenced by the channel. Hence, this paper focuses specifically on the channel MSD.

If an optimal quantization codebook is designed to minimize the source distortion, every quantized codeword will be the centroid of its corresponding quantization cell [25]. That is, $\mathbf{y}_i = \mathbf{c}_i, \forall i$. Furthermore, if the quantizer forms a matched equiprobable pair with the source, as in [20], [41], the probabilities of the quantized outputs will be $P_i = 1/M^L, \forall i$. For this equiprobale scenario, the channel MSD is

$$D_C = \frac{1}{M^L} \sum_{i=0}^{M^L-1} \sum_{j=0}^{M^L-1} P\big(\mathbf{y}_j|\mathbf{y}_i\big) \|\mathbf{y}_i - \mathbf{y}_j\|^2. \tag{6}$$

B. M-ARY INDEX ASSIGNMENT

Let us define $\mathcal{S} = \{\mathbf{s}_0, \ldots, \mathbf{s}_{M^L-1}\}$ as the set of M-ary index vectors, each with length L. Each vector $\mathbf{s}_i = [s_{i,0}, s_{i,1}, \ldots, s_{i,L-1}]^\top$ in $\mathcal{S}$ represents the M-ary expansion of integer i, i.e., $\mathbf{s}_i \in \{0, 1, \ldots, M-1\}^L$ and

$$i = \sum_{l=0}^{L-1} s_{i,l} M^{L-1-l}, \quad i = 0, 1, \ldots, M^L - 1. \tag{7}$$

The IA is described using a bijective mapping $\boldsymbol{\pi} = [\pi_0, \ldots, \pi_{M^L-1}]^\top$, where $\pi_i \in \{0, \ldots, M^L - 1\}$ represents the mapping between the quantized codeword $\mathbf{y}_{\pi_i} \in \mathcal{Y}$ and index vector $\mathbf{s}_i \in \mathcal{S}$. The communication system, depicted in Fig. 1, comprises an M^L-point equiprobable vector quantizer and an M-ary IA. The process of the system begins with an input source vector $\mathbf{x}$, which is quantized to a codeword $\mathbf{y}_{\pi_i}$. The IA mapping $\boldsymbol{\pi}$ is then used to map $\mathbf{y}_{\pi_i}$ to an index vector $\mathbf{s}_i$. The index symbols in $\mathbf{s}_i$, namely $s_{i,0}, s_{i,1}, \ldots, s_{i,L-1}$, are transmitted individually over an M-ary DMC. For example, the DMC can be resulted from modulating every index symbol into an M-ary channel symbol and transmitting it through

a memoryless channel. At the receiver, the most likely transmitted index vector is detected based on the received signals, and the corresponding quantized codeword is reconstructed using the inverse mapping of the IA. As the IA mapping is bijective, we have $P(\mathbf{y}_{\pi_j}|\mathbf{y}_{\pi_i}) = P(\mathbf{s}_j|\mathbf{s}_i)$, which allows us to express the channel MSD as

$$D_C = \frac{1}{M^L} \sum_{i=0}^{M^L-1} \sum_{j=0}^{M^L-1} P(\mathbf{s}_j|\mathbf{s}_i) \|\mathbf{y}_{\pi_i} - \mathbf{y}_{\pi_j}\|^2. \tag{8}$$

The objective of the optimal IA problem is to find the mapping $\boldsymbol{\pi}$ that minimizes the channel MSD over all possible bijective mappings between the sets $\mathcal{Y}$ and $\mathcal{S}$.

C. M-ARY LATTICE VECTOR QUANTIZER

In this study, we focus on a class of M-ary lattice quantizers defined by the following definition. These quantizers generalize the binary lattice quantizers studied in [20], [37] and can also be viewed as multistage quantizers [38] with M codewords at each stage. Therefore, the investigation of these quantizers is of both theoretical and practical interest. Our main focus in this paper is on the k-dimensional generalized lattice vector quantizers, and the scalar version can be obtained by setting k to 1.

Definition 1: Suppose that $\mathbf{B} = [\mathbf{b}_0, \mathbf{b}_1, \ldots, \mathbf{b}_{M^L-1}]$ is an $L \times M^L$ matrix consisting of M^L distinct columns $\mathbf{b}_i \in \{0, 1, \ldots, M-1\}^L$, where $i = 0, 1, \ldots, M^L - 1$. The set $\{\boldsymbol{\alpha}_0, \boldsymbol{\alpha}_1, \ldots, \boldsymbol{\alpha}_{L-1}\}$ is defined as a generating set, where $\boldsymbol{\alpha}_j \in \mathbb{R}^k$ for $j = 0, 1, \ldots, L-1$. The k-dimensional generalized M-ary lattice vector quantizer is constructed with its codebook $\mathcal{Y} = \{\mathbf{y}_0, \mathbf{y}_1, \ldots, \mathbf{y}_{M^L-1}\}$ given by

$$\mathbf{y}_i = \mathbf{y}_0 + \sum_{j=0}^{L-1} \boldsymbol{\alpha}_j B(j, i), \quad i = 0, 1, \ldots, M^L - 1, \tag{9}$$

where $\mathbf{y}_0 \in \mathbb{R}^k$.

Remark 1: The widely used uniform scalar quantizer [35] is a special case of the aforementioned lattice quantizer. By setting $k = 1$ and $\alpha_i = M^{L-1-i}\Delta$ for $i = 0, 1, \ldots, L-1$, and arranging the columns of $\mathbf{B}$ in increasing lexicographic order (c.f. Appendix C (1)), the lattice quantizer reduces to a uniform scalar quantizer with quantization step size Δ.

The M-ary lattice quantizer is of interest due to its robustness against channel noise, especially when the exact level of the channel noise is not perfectly known. To verify this property, we evaluate the performance of three vector quantizers: an unstructured vector quantizer designed to minimize source MSD (i.e., the source-optimized quantizer), a proposed M-ary lattice quantizer trained to minimize source MSD, and a channel-optimized vector quantizer [42] designed with a channel SNR of 4 dB. We use M-PAM symbols to label the quantized codewords and transmit them over an AWGN channel. In the simulations, source data are grouped into k-dimensional vectors and quantized using the three quantizers, respectively. We use the signal-to-distortion ratio (SDR)

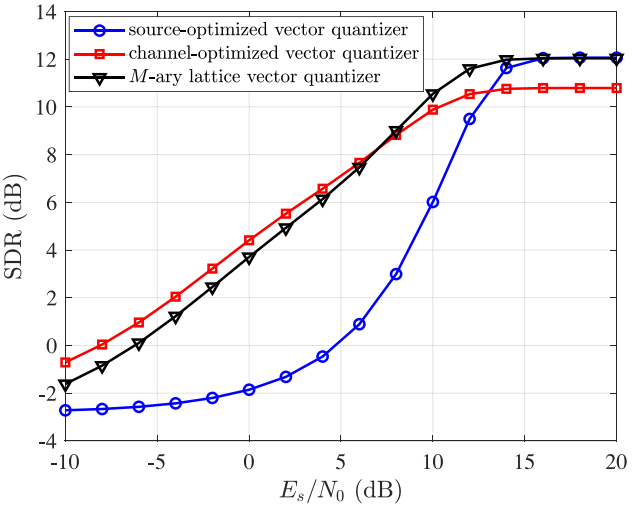

(a) SDR performance for uniform source over $[-1, 1]$.

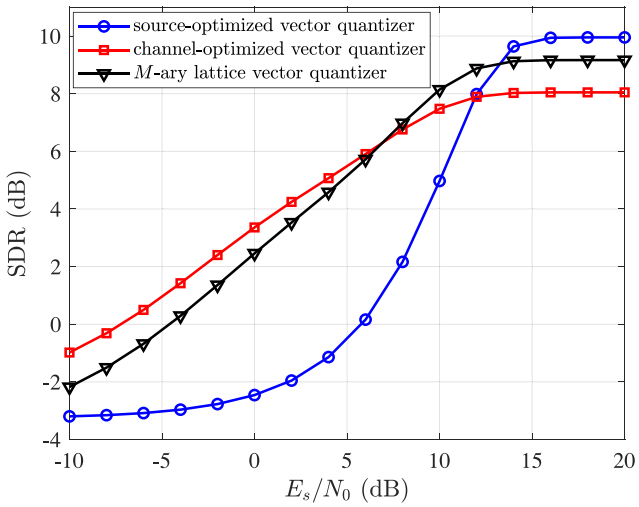

(b) SDR performance for memoryless Gaussian source with mean $\mu = 0$ and variance $\sigma^2 = 1$.

FIGURE 2. Comparison of SDR performance for three 3-dimensional 64-point vector quantizers: the source-optimized quantizer, the channel-optimized quantizer, and the 4-ary lattice quantizer. Source data are grouped as 3-dimensional vectors and quantized by the quantizers. Quantized codewords are labeled by 4-ary index vectors, and index symbols are modulated as 4-PAM symbols before being transmitted over an AWGN channel.

as the performance measure to assess the impact of source and channel MSD. Here, the SDR is defined as

$$SDR = 10 \log_{10}\left(\frac{\sigma^2}{D/k}\right), \tag{10}$$

where σ^2 is the variance of the source, and D is the overall MSD. The simulation results for uniform and Gaussian sources are shown in Fig. 2. For uniform sources, the lattice quantizer performs identically to the source-optimized quantizer at high SNRs. This is because the lattice quantizer is optimal in terms of source MSD for uniform sources. For Gaussian sources, the lattice quantizer achieves lower SDR than the source-optimized quantizer at very high SNR regions. For both types of sources, the lattice quantizers perform much better at not-too-high SNR regions

than source-optimized quantizers. Compared to the channel-optimized quantizer, the lattice quantizers perform better at high SNR regions and slightly worse when the SNR is lower than 4 dB. These results demonstrate the robustness of the M-ary lattice quantizers. Furthermore, the lattice structure reduces the implementation complexity of the quantizer [36], making it a more practical option than the other two quantizers.

III. INDEX ASSIGNMENT FOR EQUIPROBABLE LATTICE QUANTIZERS

In this section, we derive a lower bound on the channel MSD. We then propose a novel IA structure that is generalized from the optimal NBC for binary lattice quantizers. The generalized IA structure effectively transforms the IA problem into a simplified mapping problem for modulation and enables a two-step design. By designing the modulation mapping to narrow the gap between the derived lower bound and the channel MSD, our proposed approach results in near-optimal IA schemes.

To facilitate a better understanding of our design approach, we provide a running example that will be discussed in Sections III-C and IV-B. This example serves as an illustration to exemplify the relevant content.

Example 1: In a communication system, we consider a 2-dimensional 64-point lattice vector quantizer with $M = 8$ and $L = 2$, where the codebook is constructed using the matrix

$$\mathbf{B} = \begin{bmatrix} 0, & 0, & 0, & 0, \ldots, & 7, & 7, & 7, & 7 \\ 0, & 1, & 2, & 3, \ldots, & 4, & 5, & 6, & 7 \end{bmatrix},$$

and the generating set $\{\boldsymbol{\alpha}_0, \boldsymbol{\alpha}_1\}$ given by

$$\boldsymbol{\alpha}_0 = \begin{bmatrix} 2 \\ 1 \end{bmatrix}, \quad \boldsymbol{\alpha}_1 = \begin{bmatrix} 0 \\ \sqrt{3} \end{bmatrix}.$$

We set $\mathbf{y}_0 = \mathbf{0}$. The quantized data are modulated as 8-PSK symbols and transmitted over the channel. To represent all the quantized codewords using 8-PSK symbols, we need to design an IA that maps each codeword to two PSK symbols. This assignment problem is intractable due to the large number (64!) of possible candidates to compare. Therefore, we need to find an efficient way to solve this problem.

A. LOWER BOUND ON CHANNEL MEAN-SQUARED DISTORTION

Let us define the average of the codewords in $\mathcal{Y}$ by

$$\bar{\mathbf{y}} = \frac{1}{M^L} \sum_{i=0}^{M^L-1} \mathbf{y}_i.$$

According to the definition of the channel MSD in (6), the channel MSD can be rewritten as

$$D_C = \frac{1}{M^L} \sum_{i=0}^{M^L-1} \sum_{j=0}^{M^L-1} P(\mathbf{y}_j|\mathbf{y}_i) \|(\mathbf{y}_i - \bar{\mathbf{y}}) - (\mathbf{y}_j - \bar{\mathbf{y}})\|^2.$$

We can define a $k \times M^L$ matrix

$$\mathbf{Z} = \left[\mathbf{y}_{\pi_0} - \bar{\mathbf{y}}, \mathbf{y}_{\pi_1} - \bar{\mathbf{y}}, \ldots, \mathbf{y}_{\pi_{M^L-1}} - \bar{\mathbf{y}}\right],$$

where the i-th column of $\mathbf{Z}$ is $\mathbf{y}_{\pi_i} - \bar{\mathbf{y}}$. Based on [16], we rewrite the channel MSD as

$$D_C = \frac{1}{M^L} \mathrm{Tr}\left(\mathbf{Z}\mathbf{G}\mathbf{Z}^\top\right), \tag{11}$$

where $\mathbf{G}$ is a symmetric matrix corresponding to the transition probabilities, given by

$$\mathbf{G} \triangleq \sum_{i=0}^{M^L-1} \sum_{j=0}^{M^L-1} P(\mathbf{s}_j|\mathbf{s}_i)(\mathbf{e}_i - \mathbf{e}_j)(\mathbf{e}_i - \mathbf{e}_j)^\top, \tag{12}$$

where $\mathbf{e}_i$ is a column vector with 1 in position i and 0s elsewhere. It is noteworthy that the sum of each row or column of $\mathbf{G}$ is 0, as the sum of each row or column of $(\mathbf{e}_i - \mathbf{e}_j)(\mathbf{e}_i - \mathbf{e}_j)^\top$ is always 0 for any i and j.

Through the eigendecomposition of $\mathbf{G}$, we propose a lower bound on the channel MSD in the form of the following proposition.

Proposition 1: Let $\mathbf{G}$ be defined by (12), and let $\mu_{\min(2)}$ denote the second-smallest eigenvalue of $\mathbf{G}$. For an M^L-point equiprobable quantizer with quantized codewords $\{\mathbf{y}_0, \mathbf{y}_1, \ldots, \mathbf{y}_{M^L-1}\}$, a lower bound on channel MSD is

$$D_C \geq \frac{1}{M^L} \mu_{\min(2)} \sum_{i=0}^{M^L-1} \left\| \mathbf{y}_i - \frac{1}{M^L} \sum_{j=0}^{M^L-1} \mathbf{y}_j \right\|^2. \tag{13}$$

Proof: Let $\mathbf{z}_l^\top$ denote the l-th row of $\mathbf{Z}$, where $l = 0, \ldots, k-1$. Based on the trace function property (c.f. Appendix C (2)), the channel MSD in (11) can be expressed as

$$D_C = \frac{1}{M^L} \sum_{l=0}^{k-1} \mathbf{z}_l^\top \mathbf{G} \mathbf{z}_l = \frac{1}{M^L} \sum_{l=0}^{k-1} \mathrm{Tr}\left(\mathbf{G}\mathbf{z}_l\mathbf{z}_l^\top\right).$$

Let us define $\mathbf{D}_l = \mathbf{z}_l\mathbf{z}_l^\top$. Note that the sum of each row or column of $\mathbf{D}_l$ is always 0 since $\sum_{i=0}^{M^L-1}(\mathbf{y}_i - \bar{\mathbf{y}}) = \mathbf{0}$. By performing eigendecomposition on $\mathbf{G}$ and $\mathbf{D}_l$, we obtain $\mathbf{G} = \mathbf{U}\boldsymbol{\Gamma}\mathbf{U}^\top$ and $\mathbf{D}_l = \mathbf{W}_l\boldsymbol{\Omega}_l\mathbf{W}_l^\top$, where $\boldsymbol{\Gamma}$ and $\boldsymbol{\Omega}_l$ are diagonal matrices consisting of the eigenvalues of $\mathbf{G}$ and $\mathbf{D}_l$, respectively. The matrices $\mathbf{U}$ and $\mathbf{W}_l$ consist of eigenvectors of $\mathbf{G}$ and $\mathbf{D}_l$ as their columns, respectively. Using these matrices, the channel MSD can be rewritten as

$$D_C = \frac{1}{M^L} \sum_{l=0}^{k-1} \mathrm{Tr}\left(\mathbf{U}\boldsymbol{\Gamma}\mathbf{U}^\top\mathbf{W}_l\boldsymbol{\Omega}_l\mathbf{W}_l^\top\right).$$

We introduce a matrix $\boldsymbol{\Psi}_l$ defined as $\boldsymbol{\Psi}_l = \mathbf{U}^\top\mathbf{W}_l$. Note that $\boldsymbol{\Psi}_l$ is a unitary matrix since $\boldsymbol{\Psi}_l\boldsymbol{\Psi}_l^\top = \mathbf{U}^\top\mathbf{W}_l\mathbf{W}_l^\top\mathbf{U} = \mathbf{I}$. With this, the channel MSD can be expressed as

$$\begin{aligned} D_C &= \frac{1}{M^L} \sum_{l=0}^{k-1} \mathrm{Tr}\left(\boldsymbol{\Gamma}\boldsymbol{\Psi}_l\boldsymbol{\Omega}_l\boldsymbol{\Psi}_l^\top\right) \\ &= \frac{1}{M^L} \sum_{l=0}^{k-1} \sum_{i=0}^{M^L-1} \sum_{j=0}^{M^L-1} \mu_i \omega_{l,j} \Psi_l(i,j)^2, \end{aligned} \tag{14}$$

where μ_i and $\omega_{l,j}$ represent the i-th eigenvalue in $\mathbf{\Gamma}$ and the j-th eigenvalue in $\mathbf{\Omega}_l$, respectively. By relaxing the problem of minimizing (14), an optimization problem can be formulated as

$$\begin{aligned}\min_{\mathbf{\Psi}_0,\ldots,\mathbf{\Psi}_{k-1}} \quad & \sum_{l=0}^{k-1}\sum_{i=0}^{M^L-1}\sum_{j=0}^{M^L-1}\mu_i\omega_{l,j}\Psi_l(i,j)^2 \\ \text{s.t.} \quad & \sum_{i=1}^{M^L-1}\Psi_l(i,j)^2=1, \quad j=0,1,\ldots,M^L-1; \\ & l=0,1,\ldots,k-1, \\ & \sum_{j=1}^{M^L-1}\Psi_l(i,j)^2=1, \quad i=0,1,\ldots,M^L-1; \\ & l=0,1,\ldots,k-1.\end{aligned}$$

The eigenvalues in $\mathbf{\Gamma}$ and $\mathbf{\Omega}_l$ are assumed to be in ascending order, i.e., $\mu_i \le \mu_{i+1}$ and $\omega_{l,i} \le \omega_{l,i+1}$ for $i = 0, 1, \ldots, M^L-1, l = 0, 1, \ldots, k-1$, without loss of generality. It should be noted that $\mathbf{G}$ and $\mathbf{D}_l$ are positive semidefinite matrices [16], [43], and both matrices are symmetric with the sum of entries in each row or column equaling zero. Therefore, they have the smallest eigenvalue zero, associated with the eigenvector $\frac{1}{\sqrt{M^L}}\mathbf{1}$. The optimization problem above can be reduced to the one in [31], and its solution is given by

$$\mathbf{\Psi}_l = \begin{bmatrix} 1 & 0 & \cdots & 0 & 0 \\ 0 & 0 & \cdots & & \pm 1 \\ \vdots & & & \pm 1 & \\ 0 & & \iddots & & \\ 0 & \pm 1 & \cdots & & 0 \end{bmatrix}, \quad l = 0, 1, \ldots, k-1.$$

According to the above solution, the lower bound on channel MSD can be obtained as

$$D_C \ge \frac{1}{M^L}\sum_{l=0}^{k-1}\sum_{i=1}^{M^L-1}\mu_i\omega_{l,(M^L-i)}. \tag{15}$$

It is worth noting that $\mathbf{D}_l$ $(l = 0, 1, \ldots, k-1)$ is a rank-1 matrix with a unique non-zero eigenvalue of $\omega_{l,(M^L-1)} = \mathbf{z}_l^\top \mathbf{z}_l = \|\mathbf{z}_l\|^2$. Therefore, the lower bound in (15) can be expressed as

$$D_C \ge \frac{1}{M^L}\sum_{l=0}^{k-1}\mu_1\|\mathbf{z}_l\|^2 = \frac{1}{M^L}\mu_1\sum_{i=0}^{M^L-1}\left\|\mathbf{y}_i - \frac{1}{M^L}\sum_{j=0}^{M^L-1}\mathbf{y}_j\right\|^2. \tag{16}$$

Recall that μ_1 is the second-smallest eigenvalue of $\mathbf{G}$, that is, $\mu_1 = \mu_{\min(2)}$. Consequently, the lower bound in (16) is equivalent to (13) as presented in Proposition 1. ■

Remark 2: An eigenvalue-based lower bound on the channel MSD of symmetric channels has been proposed in [31]. The bound can be applied to arbitrary source models and quantizers. In the case of symmetric channels and equiprobable quantizers, our lower bound in (13) is identical to the one presented in [31]. In addition, our proposed bound in Proposition 1 can also be applied to asymmetric channels, showcasing its flexibility.

For the lattice quantizer stated in Definition 1, the proposed bound can be expressed as the following corollary.

Corollary 1: For an equiprobable M-ary lattice quantizer in Definition 1, the lower bound on channel MSD is

$$D_C \ge \frac{(M^2-1)\mu_{\min(2)}}{12}\sum_{i=0}^{L-1}\|\boldsymbol{\alpha}_i\|^2. \tag{17}$$

Proof: By substituting the lattice quantizer (9) into the lower bound (13), we get the sum in right-hand side as

$$\begin{aligned}&\sum_{i=0}^{M^L-1}\left\|\mathbf{y}_i - \frac{1}{M^L}\sum_{l=0}^{M^L-1}\mathbf{y}_l\right\|^2 \\ &= \sum_{i=0}^{M^L-1}\left\|\left(\mathbf{y}_0 + \sum_{j=0}^{L-1}\boldsymbol{\alpha}_j B(j,i)\right) - \frac{1}{M^L}\sum_{l=0}^{M^L-1}\left(\mathbf{y}_0 + \sum_{j=0}^{L-1}\boldsymbol{\alpha}_j B(j,l)\right)\right\|^2 \\ &= \sum_{i=0}^{M^L-1}\left\|\sum_{j=0}^{L-1}\boldsymbol{\alpha}_j B(j,i) - \sum_{j=0}^{L-1}\boldsymbol{\alpha}_j\frac{1}{M^L}\sum_{l=0}^{M^L-1}B(j,l)\right\|^2.\end{aligned}$$

Every row of $\mathbf{B}$ consists of values ranging from 0 to $M-1$, with each value appearing M^{L-1} times. By calculating the row sum of $\mathbf{B}$, we can simplify the above expression as

$$\sum_{i=0}^{M^L-1}\left\|\sum_{j=0}^{L-1}\boldsymbol{\alpha}_j\left(B(j,i) - \frac{M-1}{2}\right)\right\|^2.$$

Using the multinomial theorem (c.f. Appendix C (3)), we can expand the above expression as

$$\begin{aligned}&\sum_{i=0}^{M^L-1}\sum_{j=0}^{L-1}\left\|\boldsymbol{\alpha}_j\left(B(j,i) - \frac{M-1}{2}\right)\right\|^2 \\ &+ 2\sum_{i=0}^{M^L-1}\sum_{j=0}^{L-1}\sum_{l=j+1}^{L-1}\boldsymbol{\alpha}_j\boldsymbol{\alpha}_l^\top\left(B(j,i) - \frac{M-1}{2}\right) \\ &\times\left(B(l,i) - \frac{M-1}{2}\right).\end{aligned} \tag{18}$$

Note that the second term can be rewritten as

$$2\sum_{j=0}^{L-1}\sum_{l=j+1}^{L-1}\boldsymbol{\alpha}_j\boldsymbol{\alpha}_l^\top\sum_{i=0}^{M^L-1}\left(B(j,i) - \frac{M-1}{2}\right)\left(B(l,i) - \frac{M-1}{2}\right).$$

Let us define $\mathcal{C}_{j,m}$ as the set of column indices of $\mathbf{B}$ where the corresponding column has its j-th entry being m. Since each column of matrix $\mathbf{B}$ represents a distinct vector in the set $\{0, 1, \ldots, M-1\}^L$, every value in this set appears M^{L-1} times in each row of $\mathbf{B}$. Hence, there are M^{L-1} elements in the set $\mathcal{C}_{j,m}$. Additionally, among these M^{L-1} columns, the $L-1$ entries (excluding the j-th entry) in each column form a

distinct vector in the set $\{0, 1, \ldots, M-1\}^{L-1}$. Consequently, the l-th entries of the columns in $\mathcal{C}_{j,m}$ belong to the set $\{0, 1, \ldots, M-1\}$, and each of these entries appears M^{L-2} times. Hence, we have

$$\begin{aligned}
&\sum_{i=0}^{M^L-1}\left(B(j,i)-\frac{M-1}{2}\right)\left(B(l,i)-\frac{M-1}{2}\right)\\
&=\sum_{m=0}^{M-1}\sum_{i\in\mathcal{C}_{j,m}}\left(B(j,i)-\frac{M-1}{2}\right)\left(B(l,i)-\frac{M-1}{2}\right)\\
&=\sum_{m=0}^{M-1}\left(m-\frac{M-1}{2}\right)M^{L-2}\sum_{n=0}^{M-1}\left(n-\frac{M-1}{2}\right)\\
&=0.
\end{aligned}$$

Therefore, the second term in (18) is equal to 0. As a result, we can simplify the lower bound in (13) as

$$\begin{aligned}
D_C &\geq \frac{1}{M^L}\mu_{\min(2)}\sum_{i=0}^{M^L-1}\sum_{j=0}^{L-1}\left\|\boldsymbol{\alpha}_j\left(B(j,i)-\frac{M-1}{2}\right)\right\|^2\\
&=\frac{1}{M^L}\mu_{\min(2)}\sum_{j=0}^{L-1}\|\boldsymbol{\alpha}_j\|^2\sum_{i=0}^{M^L-1}\left(B(j,i)-\frac{M-1}{2}\right)^2.
\end{aligned}$$

By applying the sum of squares formula (c.f. Appendix C (4)), the above expression can be written as

$$D_C \geq \frac{(M^2-1)\mu_{\min(2)}}{12}\sum_{j=0}^{L-1}\|\boldsymbol{\alpha}_j\|^2.$$

Hence, the proof is complete. ∎

Let us consider a matrix $\mathbf{P}_{tr}$ with $P_{tr}(i,j) = P(\mathbf{s}_j|\mathbf{s}_i)$. This matrix, $\mathbf{P}_{tr}$, represents the transition matrix of the index vectors, and its second-largest eigenvalue is denoted by $\nu_{\max(2)}$. Note that the matrix $(\mathbf{e}_i - \mathbf{e}_j)(\mathbf{e}_i - \mathbf{e}_j)^\top$ has its (i,i)-th and (j,j)-th entries equal to 1, its (i,j)-th and (j,i)-th entries equal to -1, and all other entries equal to 0. According to (12), it can be easily seen that

$$G(i,j) = \begin{cases} \sum_{l\in\{0,\ldots,M^L-1\}\setminus\{i\}} P(\mathbf{s}_l|\mathbf{s}_i) + P(\mathbf{s}_i|\mathbf{s}_l), & \text{if } i=j,\\ -P(\mathbf{s}_j|\mathbf{s}_i) - P(\mathbf{s}_i|\mathbf{s}_j), & \text{if } i\neq j. \end{cases}$$

If the channel is symmetric, we have $P(\mathbf{s}_j|\mathbf{s}_i) = P(\mathbf{s}_i|\mathbf{s}_j)$. Substituting this into the above expression, one can get $\mathbf{G} = 2(\mathbf{I} - \mathbf{P}_{tr})$. To simplify the lower bound, we analyze the eigenvalues of $\mathbf{P}_{tr}$. Let $\mathbf{Q}_M$ represent the transition matrix of the M-ary DMC depicted in Fig. 1, where $Q_M(i,j) = P(j|i)$ for M-ary index symbols $0 \leq i,j \leq M-1$ in the index vector. The transition matrix of index vectors is obtained through successive Kronecker products of $\mathbf{Q}_M$, i.e.,

$$\mathbf{P}_{tr} = \underbrace{\mathbf{Q}_M \otimes \mathbf{Q}_M \otimes \cdots \otimes \mathbf{Q}_M}_{L \text{ times}}.$$

Let $\lambda_{\max(1)}, \lambda_{\max(2)}, \ldots, \lambda_{\max(M)}$ be the eigenvalues of matrix $\mathbf{Q}_M$ in decreasing order. Based on the fundamental property of the Kronecker product (c.f. Appendix C (5)), as $\mathbf{P}_{tr}$ is the Kronecker product of $\mathbf{Q}_M$ repeated L times, the eigenvalues of $\mathbf{P}_{tr}$ are computed by $\lambda^{(i_1)}\lambda^{(i_2)}\ldots\lambda^{(i_L)}$, where $\lambda^{(i_l)} \in \{\lambda_{\max(1)}, \lambda_{\max(2)}, \ldots, \lambda_{\max(M)}\}$. There are M^L combinations of this product, corresponding to M^L eigenvalues of $\mathbf{P}_{tr}$. It is obvious that the maximum eigenvalue among them is $\nu_{\max(1)} = \lambda^L_{\max(1)}$, and the second maximum eigenvalue is $\nu_{\max(2)} = \lambda^{L-1}_{\max(1)}\lambda_{\max(2)}$. Note that $\mathbf{Q}_M$ is a stochastic matrix with its largest eigenvalue $\lambda_{\max(1)} = 1$. Hence, we have $\nu_{\max(1)} = 1$ and $\nu_{\max(2)} = \lambda_{\max(2)}$.

Hence, the lower bound for the symmetric channel is

$$D_C \geq \frac{(M^2-1)(1-\lambda_{\max(2)})}{6}\sum_{i=0}^{L-1}\|\boldsymbol{\alpha}_i\|^2. \tag{19}$$

B. GENERALIZED NATURAL M-ARY CODE

Our objective is to design a universal IA scheme that is independent of the quantizer parameters. Note that the lower bound in (19) is a product of two independent terms: one depends solely on $\mathbf{Q}_M$ and the other depends only on the quantizer parameters $\{\boldsymbol{\alpha}_i\}_{i=0}^{L-1}$. To use the lower bound to aid in IA design, it deserves to find IA constructions that can also decouple the effects of channel errors and quantizer parameters on channel MSD. It has been established that the NBC is the optimal binary IA for BSCs when using equiprobable binary lattice quantizers [20]. Furthermore, the channel MSD can be decoupled into two independent terms. Thus, it is natural to investigate the M-ary generalization of the NBC for M-ary lattice quantizers.

For the lattice quantizer defined in Definition 1, the codeword $\mathbf{y}_i$ corresponds to the i-th column of the matrix $\mathbf{B}$. Let $\mathbf{b}_i$ denote the i-th column of $\mathbf{B}$, and let us denote an ordering $\boldsymbol{\zeta} = [\zeta_0, \zeta_1, \ldots, \zeta_{M^L-1}]^\top$ such that

$$\mathbf{b}_{\zeta_0} <_{\text{lex}} \mathbf{b}_{\zeta_1} <_{\text{lex}} \ldots <_{\text{lex}} \mathbf{b}_{\zeta_{M^L-1}},$$

where $\mathbf{x} <_{\text{lex}} \mathbf{y}$ means that $\mathbf{x}$ is smaller than $\mathbf{y}$ in the lexicographical order (c.f. Appendix C (1)). In this section, we introduce an M-ary IA that assigns $\mathbf{s}_i$ to the quantized codeword corresponding to $\mathbf{b}_{\zeta_i}$, denoted as $\mathbf{y}_{\zeta_i}$. As the M-ary IA is defined to assign $\mathbf{s}_i$ to $\mathbf{y}_{\pi_i}$, we can describe the IA mapping by the equation $\pi_i = \zeta_i$.

Example 2: Let us consider a 2-dimensional M-ary lattice quantizer with $M = 4$ and $L = 2$. The quantizer is constructed by the matrix $\mathbf{B}$ given by

$$\mathbf{B} = \begin{bmatrix} 1 & 1 & 1 & 1 & 0 & 0 & 0 & 0 & 3 & 3 & 3 & 3 & 2 & 2 & 2 & 2\\ 0 & 1 & 2 & 3 & 0 & 1 & 2 & 3 & 0 & 1 & 2 & 3 & 0 & 1 & 2 & 3 \end{bmatrix},$$

and the generating set $\{\boldsymbol{\alpha}_0, \boldsymbol{\alpha}_1\}$ given by

$$\boldsymbol{\alpha}_0 = \begin{bmatrix} 2 \\ 1 \end{bmatrix}, \quad \boldsymbol{\alpha}_1 = \begin{bmatrix} 0 \\ \sqrt{3} \end{bmatrix}.$$

Moreover, we set $\mathbf{y}_0 = \mathbf{0}$. The ordering $\boldsymbol{\zeta}$ is given by

$$\boldsymbol{\zeta} = [4, 5, 6, 7, 0, 1, 2, 3, 12, 13, 14, 15, 8, 9, 10, 11],$$

and then the corresponding IA $\boldsymbol{\pi}$ is

$$\boldsymbol{\pi} = [4, 5, 6, 7, 0, 1, 2, 3, 12, 13, 14, 15, 8, 9, 10, 11].$$

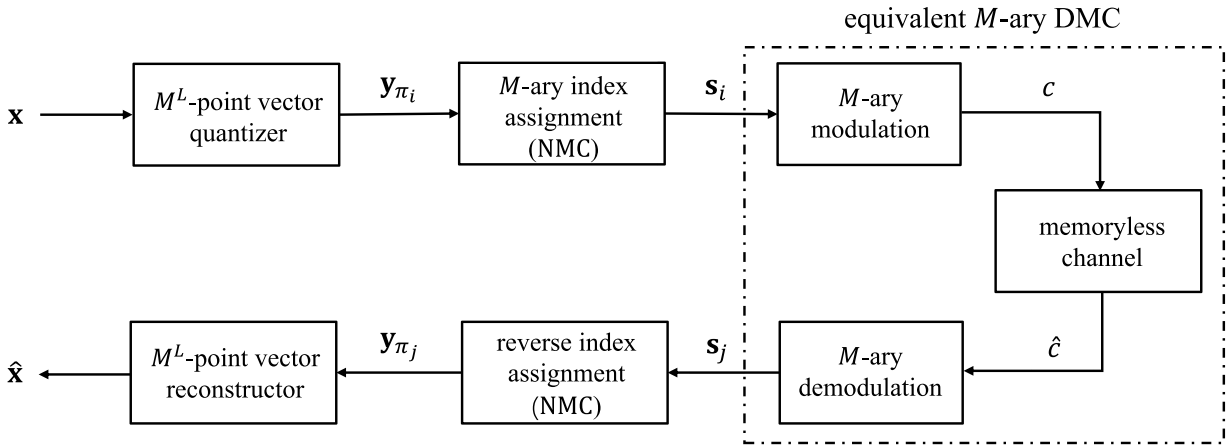

FIGURE 3. Block diagram of a communication system employing an M^L-point vector quantizer, an M-ary IA, and M-ary digital modulation.

We propose a proposition for this M-ary IA and its channel MSD, which can also serve as an upper bound on the optimal channel MSD.

Proposition 2: Suppose an M^L-point equiprobable M-ary lattice quantizer is described in Definition 1. Consider an M-ary IA defined by

$$\pi_i = \zeta_i, \quad i = 0, 1, \ldots, M^L - 1, \tag{20}$$

where ζ_i is the column index of the i-th smallest column of $\mathbf{B}$ in the lexicographic order. The channel MSD for the symmetric M-ary DMC depicted in Fig. 1, referred to as $\mathbf{Q}_M$, is given by

$$D_C = E_M \sum_{l=0}^{L-1} \|\boldsymbol{\alpha}_l\|^2, \tag{21}$$

where E_M is

$$E_M = \frac{1}{M} \sum_{i=0}^{M-1} \sum_{j=0}^{M-1} Q_M(i,j)(i-j)^2. \tag{22}$$

Proof: The proof is provided in Appendix A. ■

Consider a lattice quantizer that corresponds to a matrix $\mathbf{B}$ with the columns arranged in lexicographic order. The corresponding IA is

$$\pi_i = i, \quad i = 0, 1, \ldots, M^L - 1. \tag{23}$$

The IA is a mapping that associates the quantized codeword $\mathbf{y}_i$ with the index vector $\mathbf{s}_i$ for $i = 0, 1, \ldots, M^L-1$. This IA is referred to as the *natural M-ary code* (NMC) in this paper. It is important to note that when $M = 2$, the NBC is a specific case of the NMC. Furthermore, similar to NBC [37], NMC is a linear IA that can be implemented with low complexity, making it well-suited for applications with power-efficient requirements. For ease of discussion, we will mainly focus on the NMC throughout the rest of the paper. It is worth mentioning that any other IA described in Proposition 2 has equivalent properties to the NMC.

C. INDEX ASSIGNMENT FOR M-ARY MODULATIONS

Based on the lower bound in (19) and the channel MSD in (21), one can eliminate the influence of the quantizer parameters by computing the ratio of the two, i.e.,

$$\eta = \frac{(M^2-1)\left(1-\lambda_{\max(2)}\right)}{6E_M}. \tag{24}$$

Note that the ratio η depends on $\lambda_{\max(2)}$ and E_M, both of which are determined solely by $\mathbf{Q}_M$.

The value of η represents the gap between the lower bound and channel MSD for NMC. When η is close to 1, the gap between them is small, indicating that the proposed NMC yields near-optimal performance. It is worth noting that the IA structure only defines the mapping from quantized codewords to M-ary index vectors under the assumption that the DMC, $\mathbf{Q}_M$, is given. However, $\mathbf{Q}_M$ is dependent on the transmission of index symbols over the real channel. In order to achieve a near-optimal IA solution, it is necessary to investigate methods for transmitting index symbols over a real channel to make η close to 1. The IA solution comprises two steps, namely mapping quantized codewords to index vectors and designing a method to transmit index symbols over a real channel.

In communication systems, digital modulation schemes are often employed. Index symbols are modulated as channel symbols and then transmitted over a real channel, as depicted in Fig. 3. As shown in the figure, the modulator, the channel, and the demodulator can be grouped together and viewed as the equivalent M-ary DMC illustrated in Fig. 1. In this paper, we focus on M-ary modulations. The alphabet of M-ary index symbols is denoted by $\mathcal{I}_M = \{0, 1, \ldots, M-1\}$, and the set of M-ary channel symbols is defined as $\mathcal{C}_M = \{c_0, c_1, \ldots, c_{M-1}\}$. To describe the modulation, a bijective mapping, $\boldsymbol{\xi} = [\xi_0, \xi_1, \ldots, \xi_{M-1}]$, is defined, where $\xi_i \in \{0, 1, \ldots, M-1\}$ indicates that the index symbol $\xi_i \in \mathcal{I}_M$ is modulated as the channel symbol $c_i \in \mathcal{C}_M$.

Denote the transition matrix for channel symbols as $\hat{\mathbf{Q}}_M$, where $\hat{Q}_M(i,j) = P(c_j|c_i)$ is the probability of detecting c_j given that c_i was transmitted over the channel. Given a

modulation scheme and the channel condition, represented by $\hat{\mathbf{Q}}_M$, the transition matrix for index symbols, $\mathbf{Q}_M$, can be determined by the mapping $\boldsymbol{\xi}$, given by

$$Q_M(\xi_i, \xi_j) = \hat{Q}_M(i, j), \quad i, j = 0, 1, 2, \ldots, M-1. \quad (25)$$

Therefore, the IA problem can be addressed by designing a mapping $\boldsymbol{\xi}$ to maximize the ratio η in (24) for a given M-ary modulation scheme and channel condition. This leads to the two-step design procedure based on the NMC, as follows:

1) Label quantized codewords with M-ary index vectors using NMC.
2) Modulate index symbols as channel symbols using the mapping $\boldsymbol{\xi}$ to transmit over the real channel.

Recall the running example (c.f. Example 1) stated at the beginning of Section III. The objective is to label each quantized codeword by two PSK symbols. In the proposed two-step design, the first step involves labeling the quantized codeword using the NMC mapping, given by

$$\begin{array}{ccc} \mathcal{S} & \rightarrow & \mathcal{Y} \\ \hline [0,0] & \rightarrow & \mathbf{y}_0 \\ [0,1] & \rightarrow & \mathbf{y}_1 \\ [0,2] & \rightarrow & \mathbf{y}_2 \\ \vdots & \vdots & \vdots \\ [7,5] & \rightarrow & \mathbf{y}_{61} \\ [7,6] & \rightarrow & \mathbf{y}_{62} \\ [7,7] & \rightarrow & \mathbf{y}_{63} \end{array}, \quad (26)$$

where $\mathcal{S}$ represents the set of M-ary index vectors, where each index vector consists of M-ary index symbols, and $\mathcal{Y}$ represents the codebook for the quantizer. Note that the mapping remains independent of the generating set $\{\boldsymbol{\alpha}_j\}_{j=0}^{1}$, which highlights the generality of our proposed design.

The second step involves modulating $\mathbf{s}_i$ as two 8-PSK symbols and transmitting them over the channel. The remaining problem is to optimize $\boldsymbol{\xi}$ to maximize η.

The two-step design based on the NMC can provide optimal or near-optimal M-ary IAs for M-ary modulation schemes. In the following section, we will show that the two-step design can achieve optimal or near-optimal performance for some commonly used modulations.

IV. NEAR-OPTIMAL INDEX ASSIGNMENT SCHEMES FOR SPECIFIC *M*-ARY MODULATIONS

The M-ary modulation schemes, such as M-PAM, M-QAM, and M-PSK, are widely used in practice. As previously discussed, for a given modulation scheme, the mapping $\boldsymbol{\xi}$ that maximizes the ratio η can be found to obtain an optimal or near-optimal channel MSD performance. In this section, we will discuss the mapping problems for each of the three modulation schemes separately.

A. INDEX ASSIGNMENT SCHEME FOR PAM AND QAM

Generally, the channel matrix resulting from M-PAM transmission is asymmetric [44]. To obtain a symmetric transition matrix, we assume that erroneous signals are limited to the decision regions of the nearest neighbors of the transmitted signal, which typically occurs in high SNR scenarios [44]. Denoting the conditional transition probability as ϵ, the transition matrix for M-PAM symbols can be expressed as

$$\hat{\mathbf{Q}}_M = \begin{bmatrix} 1-\epsilon & \epsilon & 0 & \cdots & 0 \\ \epsilon & 1-2\epsilon & \epsilon & \cdots & 0 \\ \vdots & \ddots & \ddots & \ddots & \vdots \\ 0 & \cdots & \epsilon & 1-2\epsilon & \epsilon \\ 0 & \cdots & 0 & \epsilon & 1-\epsilon \end{bmatrix}. \quad (27)$$

As previously discussed, the eigenvalue of $\mathbf{Q}_M$ is important for both the mapping design and performance analysis. Thus, we present Proposition 3 for the closed-form eigendecomposition of the M-ary DMC $\mathbf{Q}_M$.

Proposition 3: Let $\mathbf{Q}_M$ be defined by the channel symbol transition matrix $\hat{\mathbf{Q}}_M$, as given in (27), and the mapping $\boldsymbol{\xi}$, as described in (25). The eigenpair $(\lambda_k, \mathbf{v}_k)$ of $\mathbf{Q}_M$ is

$$\lambda_k = 1 - 2\epsilon\left(1 - \cos\left(\frac{\pi k}{M}\right)\right), \quad k = 0, 1, \ldots, M-1, \quad (28)$$

and $\mathbf{v}_k = [v_{k,0}, v_{k,1}, v_{k,2}, \ldots, v_{k,M-1}]^\top$ in which

$$v_{k,i} = \begin{cases} \frac{1}{\sqrt{M}}, & k = 0, \\ \sqrt{\frac{2}{M}} \cos\left(\frac{\pi k}{M}\left(\phi_i + \frac{1}{2}\right)\right), & 1 \le k \le M-1, \end{cases} \quad (29)$$

where $i = 0, 1, \ldots, M-1$, and $\boldsymbol{\phi} = [\phi_0, \phi_1, \ldots, \phi_{M-1}]^\top$ denotes the inverse mapping of $\boldsymbol{\xi}$ with $\phi_{\xi_i} = i$.

Proof: Let us define $\hat{\mathbf{v}}_k = [\hat{v}_{k,0}, \hat{v}_{k,1}, \hat{v}_{k,2}, \ldots, \hat{v}_{k,M-1}]^\top$ with

$$\hat{v}_{k,i} = \begin{cases} \frac{1}{\sqrt{M}}, & k = 0, \\ \sqrt{\frac{2}{M}} \cos\left(\frac{\pi k}{M}\left(i + \frac{1}{2}\right)\right), & 1 \le k \le M-1. \end{cases}$$

It is straightforward to verify that $(\lambda_k, \hat{\mathbf{v}}_k)$ is an eigenpair of $\hat{\mathbf{Q}}_M$ by checking that $\hat{\mathbf{Q}}_M \hat{\mathbf{v}}_k = \lambda_k \hat{\mathbf{v}}_k$. According to (25), we can define a permutation matrix $\boldsymbol{\Pi}$ to represent the mapping $\boldsymbol{\xi}$ as $\hat{\mathbf{Q}}_M = \boldsymbol{\Pi} \mathbf{Q}_M \boldsymbol{\Pi}^\top$. Then we get

$$\boldsymbol{\Pi} \mathbf{Q}_M \boldsymbol{\Pi}^\top \hat{\mathbf{v}}_k = \lambda_k \hat{\mathbf{v}}_k.$$

By left-multiplying both sides of the equation by $\boldsymbol{\Pi}^\top$, we have

$$\boldsymbol{\Pi}^\top \boldsymbol{\Pi} \mathbf{Q}_M \boldsymbol{\Pi}^\top \hat{\mathbf{v}}_k = \lambda_k \boldsymbol{\Pi}^\top \hat{\mathbf{v}}_k.$$

Note that for a permutation matrix $\boldsymbol{\Pi}$, its transpose is equal to its inverse. Hence, we have $\boldsymbol{\Pi}^\top \boldsymbol{\Pi} = \mathbf{I}$ and $\boldsymbol{\Pi}^\top = \boldsymbol{\Pi}^{-1}$. The above equation can be rewritten as

$$\mathbf{Q}_M \boldsymbol{\Pi}^{-1} \hat{\mathbf{v}}_k = \lambda_k \boldsymbol{\Pi}^{-1} \hat{\mathbf{v}}_k.$$

According to the definition, $\boldsymbol{\Pi}^{-1}$ corresponds to the inverse mapping $\boldsymbol{\xi}$, namely, $\boldsymbol{\phi}$. Therefore, we have $\boldsymbol{\Pi}^{-1} \hat{\mathbf{v}}_k = \mathbf{v}_k$. Substituting this to the equation above, we get $\mathbf{Q}_M \mathbf{v}_k = \lambda_k \mathbf{v}_k$, which proves the proposition. ■

It is simple to check that the second largest eigenvalue of $\mathbf{Q}_M$ is λ_1. By substituting λ_1 into the lower bound given

in (19), the lower bound on the channel MSD for M-PAM transmission can be obtained as follows.

Corollary 2: The lower bound on channel MSD for M-PAM transmission is

$$D_C \geq \frac{(M^2-1)\epsilon}{3}\left(1-\cos\left(\frac{\pi}{M}\right)\right)\sum_{l=0}^{L-1}\|\boldsymbol{\alpha}_l\|^2. \tag{30}$$

The eigenvalues of $\mathbf{Q}_M$ are independent of the mapping $\boldsymbol{\xi}$. According to (24), finding $\boldsymbol{\xi}$ that maximizes η is equivalent to finding $\boldsymbol{\xi}$ that minimizes E_M. For the channel symbol transition matrix $\hat{\mathbf{Q}}_M$ in (27), E_M can be expressed as

$$\begin{aligned} E_M &= \frac{1}{M}\sum_{i=0}^{M-1}\sum_{j=0}^{M-1}\hat{Q}_M(i,j)(\xi_i-\xi_j)^2 \\ &= \frac{1}{M}\sum_{i=0}^{M-1}\sum_{\substack{0\leq j\leq M-1,\\ |j-i|=1}}\epsilon(\xi_i-\xi_j)^2 \\ &\overset{(a)}{\geq} \frac{1}{M}\sum_{i=0}^{M-1}\sum_{\substack{0\leq j\leq M-1,\\ |j-i|=1}}\epsilon. \end{aligned}$$

The equality in (a) holds if $(\xi_i-\xi_j)^2=1$ for $|j-i|=1$. In other words, E_M is minimized by the *identical mapping* given by

$$\xi_i = i, \quad i=0,1,2,\ldots,M-1. \tag{31}$$

By combining the NMC and the identical mapping, we obtain the *NMC-identical* scheme, which serves as the M-ary IA scheme for M-PAM transmission. The quantized codewords of the M^L-point quantizer are labeled using M-ary index vectors following the NMC, and then, M-ary index symbols are mapped to M-PAM symbols based on the identical mapping. The channel MSD associated with the NMC-identical scheme can be obtained as

$$D_C = \frac{2(M-1)\epsilon}{M}\sum_{l=0}^{L-1}\|\boldsymbol{\alpha}_l\|^2. \tag{32}$$

Based on (30) and (32), the ratio η for the NMC-identical scheme can be obtained as

$$\eta = \frac{1}{6}M(M+1)\left(1-\cos\left(\frac{\pi}{M}\right)\right). \tag{33}$$

For $M=2,3$, the ratio $\eta=1$, indicating the optimality of the NMC-identical scheme. When $M>3$, the NMC-identical scheme is suboptimal in terms of channel MSD performance. However, for practical values of M, such as 4, 8, and 16, the scheme is near-optimal, with values of η being 0.98, 0.91, and 0.87, respectively. Although η decreases as M increases, it is lower-bounded by $\frac{\pi^2}{12}$, guaranteeing the near-optimality of the NMC-identical scheme even for big values of M.

Assuming M is a power of two, we compare the proposed NMC-identical scheme to the conventional binary IA scheme. For the case of M-ary lattice quantizers and the optimal NBC applied to the BSC, we have Proposition 4 that provides the channel MSD.

Proposition 4: Given an M^L-point equiprobable M-ary lattice quantizer defined in Definition 1, and assuming the crossover probability of the BSC as p, the channel MSD corresponding to NBC is

$$D_C = \frac{p(M^2-1)}{3}\sum_{l=0}^{L-1}\|\boldsymbol{\alpha}_l\|^2. \tag{34}$$

Proof: Assume M is a power of 2. An M-ary lattice quantizer with M^L quantized codewords is equivalent to a binary lattice quantizer with $2^{L'}$ quantized codewords, where $L'=L\log_2 M$. To prove this fact, we should find a generating set $\{\boldsymbol{\alpha}'_i\}_{i=0}^{L'-1}$ and the $L'\times M^L$ matrix $\mathbf{B}'=[\mathbf{b}'_0,\mathbf{b}'_1,\ldots,\mathbf{b}'_{M^L-1}]$ that consists of M^L distinct column with $\mathbf{b}'_i\in\{0,1\}^{L'}$, $i=0,1,\ldots,M^L-1$. The lattice quantizer defined in Definition 1 is constructed by

$$\mathbf{y}_i=\mathbf{y}_0+\sum_{j=0}^{L-1}\boldsymbol{\alpha}_j B(j,i)=\mathbf{y}_0+\sum_{j=0}^{L'}\boldsymbol{\alpha}'_j B'(j,i), \tag{35}$$

for $i=0,1,\ldots,M^L-1$. The equality in (35) holds when we have $\mathbf{B}'$ and $\{\boldsymbol{\alpha}'_i\}_{i=0}^{L'-1}$ satisfy the equalities

$$\begin{cases} B(j,i)=\sum_{l=0}^{\log_2 M-1}2^{\log_2 M-1-l}B'\left(j\log_2 M+l,i\right), \\ \boldsymbol{\alpha}'_{j\log_2 M+l}=2^{\log_2 M-1-l}\boldsymbol{\alpha}_j, \end{cases} \tag{36}$$

for $i=0,1,\ldots,M^L-1$, $j=0,1,\ldots,L-1$, and $l=0,1,\ldots,\log_2 M-1$. Note that the first equation in (36) is a binary expansion of $B(j,i)$. Hence, one can always find $\mathbf{B}'$ and $\{\boldsymbol{\alpha}'_i\}_{i=0}^{L'-1}$ that satisfy the two equations in (36), which means that any M-ary lattice quantizer can be transformed into a binary lattice quantizer. Additionally, as Proposition 1 indicates, the channel MSD for NBC can be expressed as

$$D_C = p\sum_{l=0}^{L\log_2 M-1}\|\boldsymbol{\alpha}'_l\|^2=\frac{p(M^2-1)}{3}\sum_{l=0}^{L-1}\|\boldsymbol{\alpha}_l\|^2.$$

Hence, the proposition is proved. ■

Example 3: To facilitate the comprehension of Proposition 4 and its proof, we provide a simple example. Consider an M-ary lattice quantizer with $M=4$ and $L=2$, which is constructed by

$$\mathbf{B}=\begin{bmatrix}0&0&0&\cdots&3&3&3\\0&1&2&\cdots&1&2&3\end{bmatrix},$$

and

$$\boldsymbol{\alpha}_0=\begin{bmatrix}2\\1\end{bmatrix},\quad \boldsymbol{\alpha}_1=\begin{bmatrix}0\\\sqrt{3}\end{bmatrix},$$

and $\mathbf{y}_0=\mathbf{0}$. Its codebook is identical to the binary lattice quantizer with $M'=2$ and $L'=4$, which is constructed by

$$\mathbf{B}'=\begin{bmatrix}0&0&0&\cdots&1&1&1\\0&0&0&\cdots&1&1&1\\0&0&1&\cdots&0&1&1\\0&1&0&\cdots&1&0&1\end{bmatrix},$$

and

$$\boldsymbol{\alpha}'_0 = \begin{bmatrix} 4 \\ 2 \end{bmatrix}, \quad \boldsymbol{\alpha}'_1 = \begin{bmatrix} 2 \\ 1 \end{bmatrix}, \quad \boldsymbol{\alpha}'_2 = \begin{bmatrix} 0 \\ 2\sqrt{3} \end{bmatrix}, \quad \boldsymbol{\alpha}'_3 = \begin{bmatrix} 0 \\ \sqrt{3} \end{bmatrix}.$$

According to (21), the channel MSD can be computed by

$$D_C = p \sum_{l=0}^{3} \|\boldsymbol{\alpha}'_l\|^2 = \frac{p(M^2-1)}{3} \sum_{l=0}^{1} \|\boldsymbol{\alpha}_l\|^2.$$

Conventionally, binary IA is applied to M-ary modulations by mapping index bits to modulated symbols. In this approach, a BSC is modeled by considering the BER as the crossover probability. To minimize BER, binary Gray code is used in the modulation process. This results in the use of the NBC-Gray scheme. For ease of analysis, it is assumed that the resulting binary channel is ideally memoryless. Under this assumption, the crossover probability of the BSC resulting from M-PAM transmission is calculated as $p = \frac{2(M-1)}{M \log_2 M}\epsilon$ [44]. The channel MSD for the NBC-Gray scheme is

$$D_C = \frac{2(M^2-1)(M-1)\epsilon}{3M \log_2 M} \sum_{l=0}^{L-1} \|\boldsymbol{\alpha}_l\|^2. \tag{37}$$

Let us define τ as the ratio of channel MSD of the NBC-Gray scheme to the NMC-identical scheme. According to (32) and (37), the ratio τ is

$$\tau = \frac{M^2-1}{3 \log_2 M}. \tag{38}$$

This ratio is greater than 1 when $M > 2$ and continues to increase with M. This result demonstrates the superiority of the proposed M-ary IA over the binary IA for M-PAM transmission.

Remark 3: The M-QAM constellation can be decomposed into two independent $\sqrt{M}$-PAM constellations. The M-QAM mapping problem can be broken down into the labeling of an M-ary index symbol by two $\sqrt{M}$-ary index symbols, followed by the modulation of these symbols using two independent $\sqrt{M}$-PAM. Hence, the M-QAM mapping scheme is established by adopting the identical mapping for both of the $\sqrt{M}$-PAMs. Therefore, the discussions regarding M-QAM can be simplified to $\sqrt{M}$-PAM and will not be further discussed in this paper.

B. INDEX ASSIGNMENT SCHEME FOR PSK

For an additive noise channel with a PDF of noise that is symmetrically decreasing (e.g., an AWGN channel), the transition matrix $\hat{\mathbf{Q}}_M$ for M-PSK symbols satisfies the following conditions

$$\begin{cases} \sum_{i=0}^{M-1} \hat{Q}_M(i,j) = \sum_{j=0}^{M-1} \hat{Q}_M(i,j) = 1, \\ \hat{Q}_M(i,j) > \hat{Q}_M(i',j'), \quad d(i,j) < d(i',j'), \\ \hat{Q}_M(i,j) = \hat{Q}_M(i',j'), \quad d(i,j) = d(i',j'), \end{cases} \tag{39}$$

where $0 \le i, j, i', j' \le M-1$, and

$$d(i,j) = \min\{|i-j|, M-|i-j|\}$$

is the Lee distance [45]. We have Proposition 5 for the eigendecomposition of the M-ary DMC (i.e., $\mathbf{Q}_M$).

Proposition 5: Let $\mathbf{Q}_M$ be determined by the channel matrix $\hat{\mathbf{Q}}_M$ in (39) and the mapping $\boldsymbol{\xi}$ according to (25). The eigenpair $(\lambda_k, \mathbf{v}_k)$ of $\mathbf{Q}_M$ is

$$\lambda_k = \sum_{j=0}^{M-1} Q_M(i,j) \cos\left(\frac{2\pi k}{M}(\phi_j - \phi_i)\right), \quad k = 0, \ldots, M-1, \tag{40}$$

which is independent of the value $0 \le i \le M-1$, and $\mathbf{v}_k = [v_{k,0}, v_{k,1}, v_{k,2}, \ldots, v_{k,M-1}]^\top$ in which

$$v_{k,l} = \begin{cases} \frac{1}{\sqrt{M}}, & k = 0, \\ \sqrt{\frac{2}{M}} \cos\left(\frac{2\pi k}{M}\phi_l\right), & 1 \le k < \frac{M}{2}, \\ \frac{1}{\sqrt{M}}(-1)^{\phi_l}, & k = \frac{M}{2}, \\ \sqrt{\frac{2}{M}} \sin\left(\frac{2\pi k}{M}\phi_l\right), & \frac{M}{2} < k \le M-1, \end{cases} \tag{41}$$

where $0 \le l \le M-1$, and $\boldsymbol{\phi} = [\phi_0, \phi_1, \ldots, \phi_{M-1}]^\top$ denotes the inverse mapping of $\boldsymbol{\xi}$ with $\phi_{\xi_l} = l$.

Proof: Proposition 5 can be proven using a similar procedure as Proposition 3, and the proof is omitted here for brevity. ■

In order to calculate the lower bound on the channel MSD, it is necessary to find the second-largest eigenvalue of $\mathbf{Q}_M$. To achieve this, we present Corollary 3.

Corollary 3: In Proposition 5, λ_1 is the second-largest eigenvalue of $\mathbf{Q}_M$.

Proof: The proof is presented in Appendix B. ■

The lower bound on the channel MSD of M-PSK transmission is obtained as stated in the following corollary by substituting λ_1 into the lower bound in (19).

Corollary 4: The lower bound on channel MSD for M-PSK transmission is

$$\begin{aligned} D_C &\ge \frac{M^2-1}{6}\left(1 - \sum_{j=0}^{M-1} Q_M(i,j) \cos\left(\frac{2\pi}{M}(\phi_j - \phi_i)\right)\right) \sum_{l=0}^{L-1} \|\boldsymbol{\alpha}_l\|^2 \\ &= \frac{M^2-1}{6}\left(1 - \sum_{j=0}^{M-1} \hat{Q}_M(i,j) \cos\left(\frac{2\pi}{M}(j-i)\right)\right) \sum_{l=0}^{L-1} \|\boldsymbol{\alpha}_l\|^2. \end{aligned} \tag{42}$$

The optimization problem of maximizing η, as described in (24), is equivalent to finding the minimum value of E_M. This problem is similar to the optimal IA problem discussed in [33], [34] and can be solved using the *zigzag mapping*, which is given by

$$\boldsymbol{\xi}_{\text{zig}} = [0, 1, 3, \ldots, M-1, \ldots, 4, 2]. \tag{43}$$

We propose the *NMC-zigzag* scheme by combining the NMC and the zigzag mapping to serve as the M-ary IA scheme for M-PSK transmission. The NMC maps quantized codewords of the M^L-point quantizer to M-ary index vectors. The zigzag mapping then maps the M-ary index symbols to M-PSK symbols.

Recall the running example (c.f. Example 1) presented in Section III. A two-step design approach was employed for the design of M-ary IA. The first step has been solved using the mapping defined in (26). In the second step, the zigzag mapping $\boldsymbol{\pi} = [0, 1, 3, 5, 7, 6, 4, 2]$, i.e.,

$$\begin{array}{ccc} \mathcal{C}_M & \rightarrow & \mathcal{I}_M \\ \hline c_0 & \rightarrow & 0 \\ c_1 & \rightarrow & 1 \\ c_2 & \rightarrow & 3 \\ \vdots & \vdots & \vdots \\ c_5 & \rightarrow & 6 \\ c_6 & \rightarrow & 4 \\ c_7 & \rightarrow & 2 \end{array}, \tag{44}$$

where $\mathcal{C}_M$ and $\mathcal{I}_M$ denote the set of M-ary channel symbols and M-ary index symbols, respectively.

To facilitate performance analysis, we make the high SNR assumption, which means that incorrectly detected channel symbols are limited to the nearest neighbors of the transmitted symbols. As a result, we simplify $\hat{\mathbf{Q}}_M$ to the following form

$$\hat{\mathbf{Q}}_M = \begin{bmatrix} 1-2\epsilon & \epsilon & 0 & \cdots & \epsilon \\ \epsilon & 1-2\epsilon & \epsilon & \cdots & 0 \\ \vdots & \ddots & \ddots & \ddots & \vdots \\ 0 & \cdots & \epsilon & 1-2\epsilon & \epsilon \\ \epsilon & \cdots & 0 & \epsilon & 1-2\epsilon \end{bmatrix}. \tag{45}$$

Under the assumption, the channel MSD for the NMC-zigzag scheme can be obtained as

$$D_C = \frac{4(2M-3)\epsilon}{M} \sum_{l=0}^{L-1} \|\boldsymbol{\alpha}_l\|^2. \tag{46}$$

Hence, the ratio of the channel MSD to the lower bound is

$$\eta = \frac{M\left(M^2-1\right)}{12(2M-3)} \left(1 - \cos\left(\frac{2\pi}{M}\right)\right). \tag{47}$$

The NMC-zigzag scheme is demonstrated to be optimal for $M = 2, 3, 4$, as indicated by the ratio of channel MSD to the lower bound being equal to 1. Note that when $L = 1$, the scheme reduces to the IA mapping discussed in [33], [34], and it has been proven to be optimal for any value of M when $L = 1$. Though the scheme is suboptimal for $M > 4$ and $L > 2$, it still retains its near-optimality for practical values of M, with the ratio being close to 1, specifically 0.95 and 0.89 for $M = 8$ and 16, respectively. The ratio η is lower bounded by $\frac{\pi^2}{12}$, further ensuring that the NMC-zigzag scheme remains near-optimal, although η decreases with increasing M.

We also compare the NMC-zigzag scheme to the conventional binary IA scheme. The binary IA scheme uses the binary Gray code to modulate index bits to M-PSK symbols, resulting in an equivalent BSC with crossover probability $p = \frac{2}{\log_2 M}\epsilon$ [44]. The channel MSD of the binary IA scheme, namely the NBC-Gray scheme, can be computed using Proposition 4, and given by

$$D_C = \frac{2\left(M^2-1\right)\epsilon}{3\log_2 M} \sum_{l=0}^{L-1} \|\boldsymbol{\alpha}_l\|^2. \tag{48}$$

One can compare the channel MSD of the NBC-Gray and NMC-zigzag schemes for M-PSK transmission by finding the ratio between the two. This ratio is

$$\tau = \frac{M\left(M^2-1\right)}{6\log_2 M(2M-3)}. \tag{49}$$

For $M > 4$, the ratio is greater than 1 and increases with M, indicating that the M-ary IA outperforms the binary IA in channel MSD for M-PSK transmission.

C. OPTIMAL INDEX ASSIGNMENT FOR 3-PSK AND QPSK

In previous discussions, we have shown that our proposed IA schemes are optimal for specific values of M under high SNR conditions. However, for M-PSK with $M = 2, 3, 4$, the NMC-zigzag scheme is optimal even without such an assumption. The NMC-zigzag scheme is equivalent to the NBC when $M = 2$, and its optimality has been proven in [20]. For $M = 3, 4$, we provide the following theorem to demonstrate the optimality of the NMC-zigzag scheme.

Theorem 1: For an M^L-point equiprobable M-ary lattice quantizer as defined in Definition 1, the NMC-zigzag scheme is the optimal IA scheme for M-PSK when $M = 3, 4$.

Proof: A sufficient condition for the optimality is that the channel MSD achieves the lower bound, i.e., $\eta = 1$. We will prove that the DMC $\mathbf{Q}_M$ corresponding to NMC-zigzag scheme achieves $\eta = 1$ when $M = 3, 4$. Since

$$\sum_{i=0}^{M-1} Q_M(i,j) = \sum_{j=0}^{M-1} Q_M(i,j) = 1$$

holds for symmetric channels, E_M can be rewritten as

$$E_M = \frac{2}{M} \sum_{i=0}^{M-1} \left(i - \frac{M-1}{2}\right)^2 - \frac{2}{M} \sum_{i=0}^{M-1} \sum_{j=0}^{M-1} Q_M(i,j) \left(i - \frac{M-1}{2}\right)\left(j - \frac{M-1}{2}\right). \tag{50}$$

Define $\mathbf{r} = [r_0, r_1, \ldots, r_{M-1}]^\top$, where $r_i = (i - \frac{M-1}{2})$, and denote the i-th eigenpair of $\mathbf{Q}_M$ by $(\lambda_i, \mathbf{v}_i)$. Then (50) can be written as

$$\begin{aligned} E_M &= \frac{2}{M}\|\mathbf{r}\|^2 - \frac{2}{M}\mathbf{r}^\top \mathbf{Q}_M \mathbf{r} \\ &= \frac{2}{M}\|\mathbf{r}\|^2 - \frac{2}{M}\sum_{i=0}^{M-1} \lambda_i \|\mathbf{v}_i^\top \mathbf{r}\|^2 \\ &\overset{(b)}{=} \frac{2}{M}\|\mathbf{r}\|^2 - \frac{2}{M}\sum_{i=1}^{M-1} \lambda_i \|\mathbf{v}_i^\top \mathbf{r}\|^2 \\ &\overset{(c)}{\geq} \frac{2\left(1-\lambda_{\max(2)}\right)}{M}\|\mathbf{r}\|^2, \end{aligned}$$

where (b) is because $\mathbf{v}_0 = (1/\sqrt{M})\mathbf{1}$ and $\mathbf{v}_0^\top \mathbf{r} = 0$. Let $\mathbb{E}_1$ denote the eigenspace associated with the eigenvalue $\lambda_{\max(2)}$ (which comprises the zero vector and all the eigenvectors related to $\lambda_{\max(2)}$). The equality in (c) holds when we have

$$\sum_{\mathbf{v}_i \in \mathbb{E}_1} \left\| \mathbf{v}_i^\top \mathbf{r} \right\|^2 = \|\mathbf{r}\|^2. \tag{51}$$

A condition sufficient for (51) to hold is that $\mathbf{r}$ can be expressed as a linear combination of eigenvectors in the eigenspace $\mathbb{E}_1$. Proposition 5 states that the eigenvalue $\lambda_{\max(2)}$ has a multiplicity of 2, and the eigenspace $\mathbb{E}_1$ consists of two eigenvectors, $\mathbf{v}_1$ and $\mathbf{v}_{M-1}$. By defining $\mathbf{V} = [\mathbf{v}_1, \mathbf{v}_{M-1}]$, we can find coefficient vectors $\mathbf{a}$ as

$$\mathbf{a} = \begin{cases} \left[-\frac{\sqrt{6}}{2}, \frac{1}{\sqrt{2}}\right]^\top, & M = 3, \\ \left[-\frac{3}{\sqrt{2}}, \frac{1}{\sqrt{2}}\right]^\top, & M = 4, \end{cases}$$

such that $\mathbf{r} = \mathbf{V}\mathbf{a}$, implying that $\mathbf{r}$ is a linear combination of the two eigenvectors when $\mathbf{Q}_M$ corresponds to the NMC-zigzag scheme. Therefore, it can be shown that the equality in (c) holds when NMC-zigzag scheme is applied, i.e.,

$$E_M = \frac{2\big(1 - \lambda_{\max(2)}\big)}{M} \|\mathbf{r}\|^2 = \frac{\big(M^2 - 1\big)\big(1 - \lambda_{\max(2)}\big)}{6}.$$

By substituting the expression obtained above into (24), we get $\eta = 1$, which means that the channel MSD achieves the lower bound. Therefore, the optimality is proven. ■

V. NUMERICAL RESULTS

In this section, we present simulation results to demonstrate the effectiveness of our proposed schemes. We first show the performance of proposed IA schemes and compare them with the derived performance bounds and the conventional binary IA scheme. Subsequently, we introduce a WSN model and compare the energy consumption of our proposed IA scheme and the binary counterpart in the WSN application.

A. PERFORMANCE EVALUATION AND COMPARISON WITH THE PERFORMANCE BOUNDS

Though our schemes are designed to minimize the channel MSD for equiprobable M-ary lattice vector and scalar quantizers, it is worth noting that equiprobable quantizers may not always be optimal in terms of source distortion [41]. However, when the source is uniformly distributed, the optimal lattice quantizer in terms of source distortion is also equiprobable. Therefore, our simulations focus on this widely used and optimal scenario, namely, lattice vector quantizers in conjunction with uniform sources, to evaluate the proposed schemes.

Simulation results for the three modulation schemes are presented to evaluate the performance of the proposed M-ary IA schemes and to compare them with SDR bounds obtained by substituting the lower bounds on channel MSD into (10). In each simulation, real-valued source data are generated from a uniform distribution and grouped into k-dimensional vectors, which are then quantized using a k-dimensional M^L-point lattice vector quantizer optimized to minimize source distortion. The resulting quantized codewords are labeled with M-ary index vectors, which are mapped to channel symbols and transmitted over an AWGN channel. At the receiver, the detected channel symbols are demodulated back into index symbols, and the source vectors are reconstructed. The conventional binary IA scheme, namely the NBC-Gray scheme, is also evaluated, and its simulation performance is shown to demonstrate the benefits of the proposed schemes. For the simulations of the binary IA, we interleaved the index bits before modulation and de-interleaved them after demodulation to obtain an ideal memoryless BSC.

The performance of k-dimensional lattice quantizers for PAM and QAM transmissions was evaluated through simulations. To ensure a fair comparison between PAM and QAM, we used the same lattice quantizers for both modulation schemes. Note that although we refer to the quantizers of interest as "lattice quantizers", our performance analyses are not restricted to the constraint that $k \geq L$. In order to provide a more comprehensive investigation and theoretical understanding, we conduct simulations for cases where $k < L$, $k = L$, and $k > L$. For 4-PAM and 16-QAM, simulations were conducted for 256-point lattice quantizers constructed with $M = 4$, $L = 4$, and $k = 3, 4, 5$. For 8-PAM and 64-QAM, simulations were conducted for 64-point lattice quantizers constructed with $M = 8$, $L = 2$, and $k = 1, 2, 3$. The simulation results are depicted in Fig. 4 and Fig. 5. In addition, simulations were also performed for PSK transmissions, including 512-point lattice quantizers constructed with $M = 8$, $L = 3$, and $k = 2, 3, 4$ for 8-PSK, and 256-point lattice quantizers constructed with $M = 16$, $L = 2$, and $k = 1, 2, 3$ for 16-PSK. The results for PSK transmissions are depicted in Fig. 6.

The simulation results demonstrate that the proposed M-ary IA schemes achieve near-optimal performance and outperform the binary IA scheme in all simulation settings. Recall that the SDR is dependent on the overall MSD. At asymptotically high SNR levels, the source MSD becomes the dominant factor in the overall MSD, and the channel MSD is negligible. Although the proposed IA scheme exhibits superior performance in reducing channel MSD compared to the conventional one, the difference in overall MSD is negligible. Consequently, the SDR performance of both schemes converges when operating at asymptotically high SNRs. However, in scenarios where the SNR is not asymptotically high, the channel MSD has a significant contribution to the overall MSD. As the proposed IA schemes are better than the conventional binary scheme for reducing channel MSD, they achieve higher SDR performance in such regions. The SDR performance for M-PAM and M^2-QAM transmissions are identical, with the only difference being that the channel SNR required for QAM is approximately 3 dB higher than that for PAM to achieve the same SDR performance. This is because one M^2-QAM symbol can be

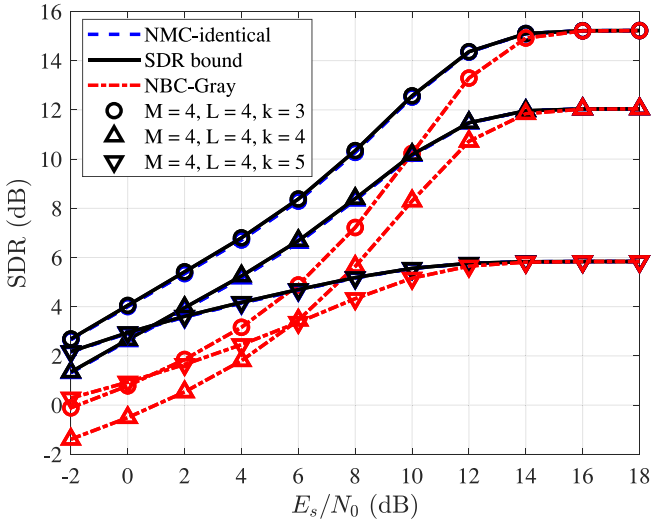

(a) Results for 4-PAM transmission.

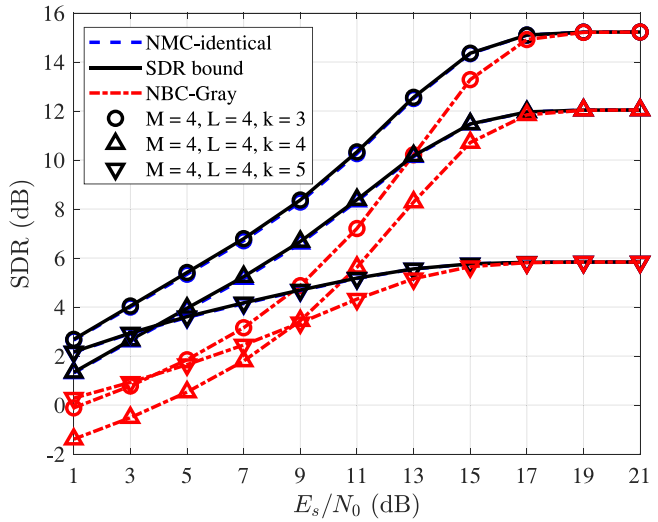

(b) Results for 16-QAM transmission.

FIGURE 4. SDR performance comparison of the NMC-identical scheme, the NBC-Gray scheme, and the SDR bound derived from (30) for PAM and QAM transmissions for k-dimensional 256-point lattice vector quantizers constructed with $M = 4$, $L = 4$, and $k = 3, 4, 5$.

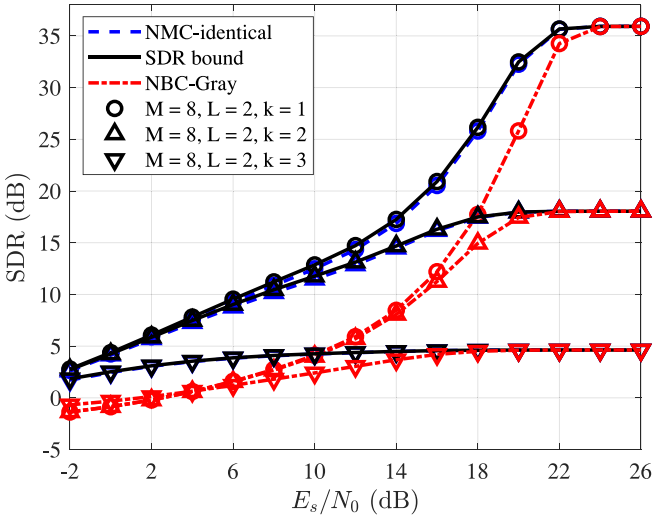

(a) Results for 8-PAM transmission.

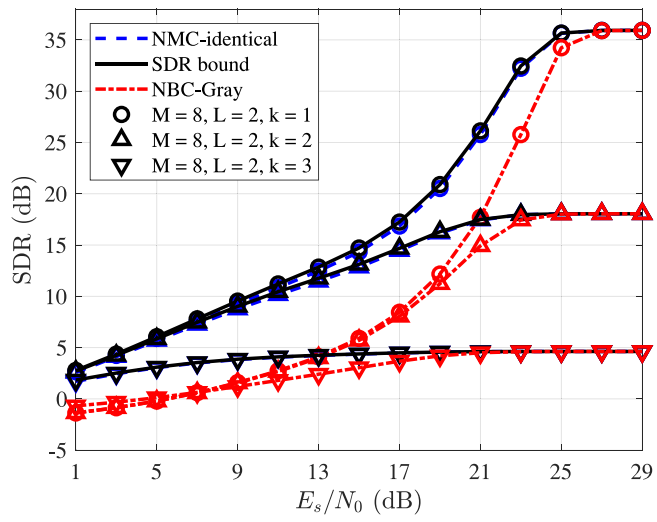

(b) Results for 64-QAM transmission.

FIGURE 5. SDR performance comparison of the NMC-identical scheme, the NBC-Gray scheme, and the SDR bound derived from (30) for PAM and QAM transmissions for k-dimensional 64-point lattice vector quantizers constructed with $M = 8$, $L = 2$, and $k = 1, 2, 3$.

viewed as two M-PAM symbols, necessitating double the transmitted symbol power to achieve equivalent performance. Furthermore, the proposed IA schemes provide significant SNR gains compared to the conventional NBC-Gray scheme, with gains of up to 5 dB and 12 dB for 4-PAM (16-QAM) and 8-PAM (64-QAM), respectively. For PSK transmission, the gains in SNR are up to 3 dB and 8 dB for 8-PSK and 16-PSK, respectively. It is noteworthy that these gains increase with the modulation orders and are particularly significant for high orders.

It is worth noting that when M and L are fixed, the SDR performance of a lattice vector quantizer decreases as the dimension k increases in not-too-small SNR regions. However, when the SNR is low enough, it is observed that the SDR performance decreases with k when $2 \leq k < L$ and then increases with k when $k \geq L$, whereas the SDR performances for $k = 1$ and $k = L$ are identical.

In high SNR regions, source MSD dominates overall MSD. When $k \leq L$, the generating set $\{\boldsymbol{\alpha}_j\}_{j=0}^{L-1}$ can span the full space of data vectors, but since the size of the quantization codebook is fixed, increasing the dimension of the lattice vector quantizer enlarges quantization cell sizes per dimension, resulting in increased source distortion. When $k > L$, the generating set cannot span the full space of data vectors, and some data vectors will be far from the quantized codewords, resulting in significant source MSD. Therefore, the source MSD per dimension increases with k.

In low enough SNR regions, the effect of channel MSD is more significant than that of the source MSD. When $k = 1$, the lattice quantizer is an M^L-level uniform scalar

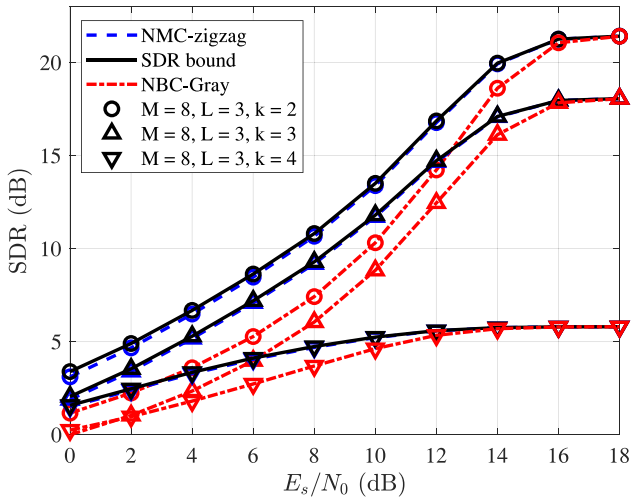

(a) Results for 512-point M-ary lattice vector quantizers constructed with $M = 8$, $L = 3$, and $k = 2, 3, 4$, and with 8-PSK.

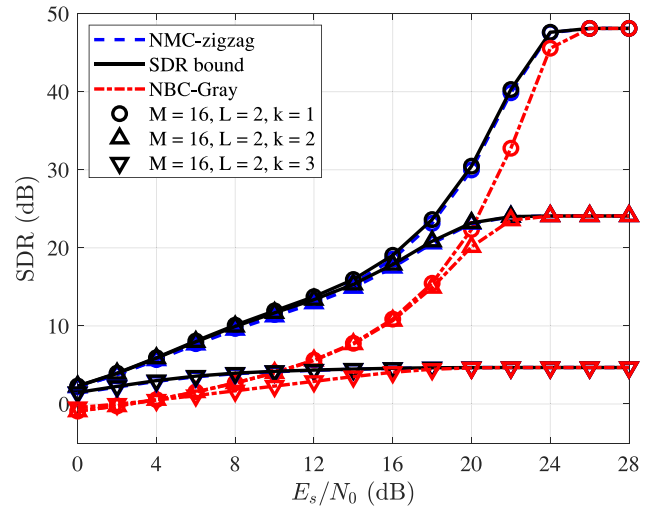

(b) Results for 256-point M-ary lattice vector quantizer constructed with $M = 16$, $L = 2$, and $k = 1, 2, 3$, and with 16-PSK.

FIGURE 6. SDR performance comparison of the NMC-zigzag scheme, the NBC-Gray scheme, and the SDR bound derived from (42) for PSK transmissions for *k*-dimensional lattice vector quantizers.

quantizer. On the other hand, the lattice quantizer with $k = L$ can be viewed as the Cartesian product of k uniform scalar quantizers, each having M quantization levels, and its channel MSD per dimension is equal to that of an M-level uniform scalar quantizer. As reported in [1], [20], uniform scalar quantizers with varying quantization levels have asymptotically equivalent channel MSDs, indicating that SDR performance for $k = 1$ and $k = L$ at low enough SNR region is the same. When $2 \leq k \leq L$, increasing k increases quantization cell sizes per dimension, causing the squared Euclidean distances per dimension between codewords also to increase, resulting in an increase in channel MSD per dimension. However, when $k > L$, the subspace spanned by the generating set does not increase as much as the dimension k, causing the squared Euclidean distances per dimension between quantized codewords to decrease, leading to a decrease in channel MSD per dimension.

The proposed IA schemes do not require complex encoding and decoding processes like those used in systems with channel codes. This makes the proposed schemes suitable for low-power, low-latency applications such as WSNs. Hence, in Section V-B, we will present experimental results for a simple WSN to showcase the potential applications of the proposed IA schemes.

B. APPLICATION IN ENERGY-EFFICIENT WIRELESS SENSOR NETWORKS

1) MODEL OF ENERGY-EFFICIENT WIRELESS SENSOR NETWORKS

To evaluate the energy consumption in a WSN, we adopt a model described in prior studies such as [46], [47]. For clarity, we will provide a brief overview of the model here, but interested readers are encouraged to consult these studies for more information. In general, a sensor node's energy consumption can be divided into three main categories: communication energy, computation energy, and sensing energy [8]. In most cases, computation and sensing energy are considered insignificant compared to communication energy [8], so we will only focus on the communication energy component. A node's transceiver is only working (i.e., in *active* mode) when sending or receiving data and is in *sleep* mode at all other times. The energy consumption per source symbol when transmitting N_s source symbols can be calculated by

$$E = \frac{P_{on}T_{on} + P_{sp}T_{sp} + P_{tr}T_{tr}}{N_s}, \tag{52}$$

where P_{on}, P_{sp}, and P_{tr} are the power consumption when the transceiver is in the active mode, the sleep mode, and the *transient* mode (switching between active and sleep modes), respectively, and T_{on}, T_{sp}, and T_{tr} are the time durations of the three modes respectively. The power consumption in the sleep mode is much lower than that in the active mode and thus can be disregarded. The power and time spent in the transient mode are constants corresponding to the given hardwares [48]. Hence, we will only consider the energy consumption in the active mode to compare the two IA schemes. This consumption is mainly composed of two components: the power P_t required for transmitting the signal and the power P_{ct} required by the radio circuit components [49]. The energy consumption per symbol can then be expressed as

$$E = \frac{(P_t + P_{ct})T_{on}}{N_s}. \tag{53}$$

The power consumption of radio circuit components, P_{ct}, is composed of various circuit components, including the power amplifier [46], [49]. The power consumption of the amplifier, P_{amp}, is proportional to the transmitted signal power P_t with $P_{\text{amp}} = \alpha P_t$, where the constant α is dependent on the modulation scheme and hardware. The remaining circuit components have power consumption independent

TABLE 1. Simulation parameters for WSN energy consumption evaluation.

$\alpha = 1.9$	$\kappa = 3.5$	$\frac{N_0}{2} = -174$ dBm/Hz	$M_l = 40$ dB
$B = 10$ kHz	$L = 2$K symbols	$G_1 = 30$ dB	$N_f = 10$ dB
$P_{\text{filt}} = 2.5$ mW	$P_{\text{mix}} = 30.3$ mW	$P_{\text{syn}} = 50$ mW	$P_{\text{LNA}} = 20$ mW
$P_{\text{filr}} = 2.5$ mW	$P_{\text{IFA}} = 3$ mW	$P_{\text{ADC}} = 4.1$ mW	$P_{\text{DAC}} = 55$ mW

of the signal power and can be combined and considered together as

$$P_c = \left(P_{\text{mix}} + P_{\text{syn}} + P_{\text{filt}} + P_{\text{DAC}}\right) + \left(P_{\text{mix}} + P_{\text{syn}} + P_{\text{LNA}} + P_{\text{filr}} + P_{\text{IFA}} + P_{\text{ADC}}\right), \quad (54)$$

where P_{mix}, P_{syn}, P_{filt}, P_{DAC}, P_{LNA}, P_{IFA}, and P_{ADC} are the power consumptions in the various circuit components [49]. The expression in the first bracket of (54) represents the power consumption of the transmitter's circuit components, whereas the expression in the second bracket represents the power consumption of the receiver's circuit components. The total energy consumption of the node can be expressed as

$$E = \frac{((1+\alpha)P_t + P_c)T_{on}}{N_s}. \quad (55)$$

The transmitted signal power P_t can be expressed with the received signal power P_r at the receiver [46], given by

$$P_t = P_r G_1 d^{\kappa} M_l, \quad (56)$$

where d is the transmission distance, G_1 represents the gain factor at the distance of $d = 1$, κ is the path loss exponent, and M_l denotes the link margin that accounts for any imperfections in the hardware process variations and noise. The received signal power in an AWGN channel can be expressed in terms of the received SNR γ per channel symbol, given by

$$P_r = \gamma B N_0 N_f, \quad (57)$$

where B is the bandwidth, $N_0/2$ is the noise spectral density for an AWGN channel, and N_f is the receiver noise figure.

The duration of the active mode, T_{on}, is determined by the modulation scheme, bandwidth, and the length of the source sequence. For a sequence of N_s data samples quantized by an M^L-point quantizer and transmitted using M-ary modulation, the active duration is given by

$$T_{on} = \frac{N_s L}{B}. \quad (58)$$

Using the equations (54) to (58), one can calculate the energy consumption of a WSN sensor node with specific circuit component and channel parameters.

2) EVALUATION OF ENERGY SAVING

To demonstrate the energy savings achieved by the proposed M-ary IA scheme compared to the conventional binary IA scheme in the WSN application, we conducted simulations to calculate the energy consumption for both IA schemes using QAM modulation. The NMC-identical scheme is adopted for the M-ary IA design, whereas the binary counterpart uses the NBC-Gray scheme. First, we obtained the corresponding received SNRs for the desired SDR performances through simulations. Then, we determined the energy consumption for the desired SDR performances based on the WSN model described in the previous subsection. In the simulation, we considered a system with a uniform source, a low-complexity analog-to-digital converter in the form of a uniform scalar quantizer, and the QAM modulation. Table 1 lists the parameters of the WSN used in the simulation.

The percentage energy saving of the NMC-identical scheme over the NBC-Gray scheme is used to compare the power consumption of the two approaches and is defined as

$$\text{Energy Saving } (\%) = \frac{E_b - E_m}{E_b} \times 100\%, \quad (59)$$

where E_m and E_b represent the energy consumption of the NMC-identical and the NBC-Gray scheme, respectively.

The results for energy savings are presented in Fig. 7, where it is shown that the proposed NMC-identical scheme is significantly more energy-efficient for M-ary transmission compared to the conventional NBC-Gray scheme. It is also noteworthy that the energy savings are more significant for longer transmission distances, as the signaling power becomes the dominant factor. In contrast, at short distances, circuit consumption dominates the overall energy consumption, resulting in similar energy consumption for both schemes.

VI. CONCLUSION

In this work, we have investigated the M-ary IA problem for equiprobable lattice quantizers and M-ary transmissions to improve energy efficiency in wireless communication. We have derived performance bounds on channel MSD and proposed explicit M-ary IA constructions for three practical M-ary modulation schemes, namely PAM, QAM, and PSK. We have compared the proposed IAs with lower bounds by introducing the ratio η and demonstrated their near-optimality by showing that η is close to 1 for practical values of M and is lower bounded by $\frac{\pi^2}{12}$. Moreover, we have proven the optimality of the NMC-zigzag scheme for M-PSK transmissions when $M = 3, 4$. We have conducted simulations to evaluate the performance of the proposed IAs under varying settings of quantizers. The results show that the proposed IAs can approach the upper bound on SDR performance with negligible gaps. The simulations also show that the proposed IAs can achieve significant SDR gains compared to the conventional binary IA, and these gains increase with M. In

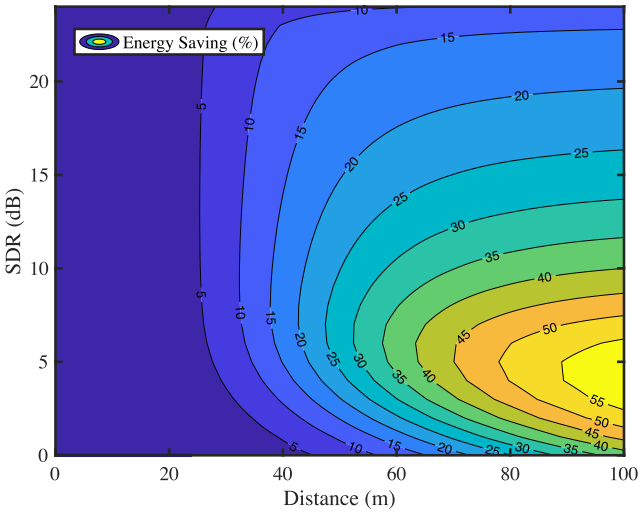

(a) Results for 16-level quantizer with 16-QAM.

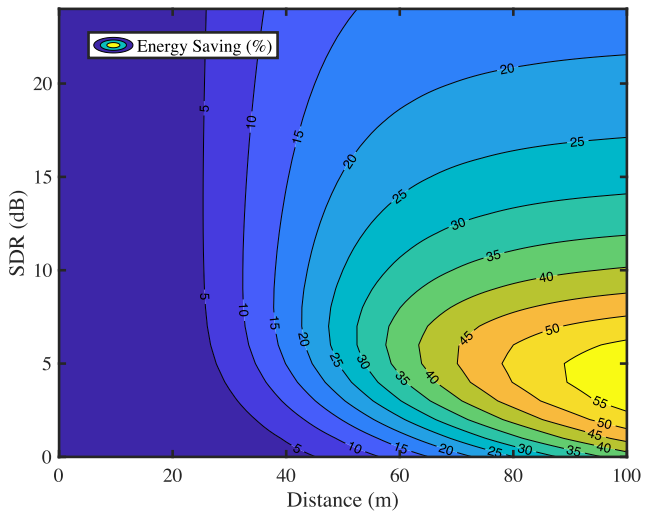

(b) Results for 256-level quantizer with 16-QAM.

FIGURE 7. Energy saving (%) of the NMC-identical scheme over the conventional binary IA scheme for the WSN application, with an equiprobable uniform scalar quantizer and 16-QAM modulation.

addition, we have demonstrated that the proposed M-ary IA can lead to significant energy savings in WSN applications, and such savings increase with the transmission distance. These results indicate that the proposed M-ary IA schemes can effectively enhance the energy efficiency of wireless communication systems. Further research on nonbinary IA for non-equiprobable or unstructured quantizers, as well as error correction coded systems, can extend our findings to more general energy-efficient wireless communication scenarios.

APPENDIX A
PROOF OF PROPOSITION 2

As per the description of IA given in Proposition 2, $\mathbf{y}_{\pi_i}$ can be computed by

$$\mathbf{y}_{\pi_i} = \mathbf{y}_{\zeta_i} = \mathbf{y}_0 + \sum_{l=0}^{L-1} \boldsymbol{\alpha}_l B(l, \zeta_i).$$

Note that $\mathbf{b}_{\zeta_i} = \mathbf{s}_i$. According to Definition 1, $\mathbf{y}_{\pi_i}$ can be computed by

$$\mathbf{y}_{\pi_i} = \mathbf{y}_0 + \sum_{l=0}^{L-1} s_{i,l}\boldsymbol{\alpha}_l,$$

and the channel MSD can be rewritten as

$$\begin{aligned} D_C &= \frac{1}{M^L}\sum_{i=0}^{M^L-1}\sum_{j=0}^{M^L-1} P(\mathbf{s}_j|\mathbf{s}_i)\left\|\mathbf{y}_{\pi_i} - \mathbf{y}_{\pi_j}\right\|^2 \\ &= \frac{1}{M^L}\sum_{i=0}^{M^L-1}\sum_{j=0}^{M^L-1} P(\mathbf{s}_j|\mathbf{s}_i)\left\|\mathbf{y}_0 + \sum_{l=0}^{L-1} s_{i,l}\boldsymbol{\alpha}_l - \mathbf{y}_0 - \sum_{l=0}^{L-1} s_{j,l}\boldsymbol{\alpha}_l\right\|^2 \\ &= \frac{1}{M^L}\sum_{i=0}^{M^L-1}\sum_{j=0}^{M^L-1} P(\mathbf{s}_j|\mathbf{s}_i)\left\|\sum_{l=0}^{L-1}(s_{i,l} - s_{j,l})\boldsymbol{\alpha}_l\right\|^2. \end{aligned} \tag{60}$$

Recall that the channel is memoryless and the index symbols in the index vector are independent. Therefore, we can use the property $P(\mathbf{s}_j|\mathbf{s}_i) = \prod_{l=0}^{L-1} P(s_{j,l}|s_{i,l})$ and substitute it into (60), which yields

$$D_C = \frac{1}{M^L}\sum_{i=0}^{M^L-1}\sum_{j=0}^{M^L-1}\prod_{l=0}^{L-1} P(s_{j,l}|s_{i,l})\left\|\sum_{l=0}^{L-1}(s_{i,l} - s_{j,l})\boldsymbol{\alpha}_l\right\|^2.$$

For the sake of notational convenience, let us denote $s_{i,0}$ and $s_{j,0}$ by s_{i_0} and s_{j_0}, respectively. With this notation, the above expression can be expanded as

$$\begin{aligned} D_C = \frac{1}{M^L}\sum_{i_0=0}^{M-1}\sum_{j_0=0}^{M-1}\sum_{i=0}^{M^{L-1}-1}\sum_{j=0}^{M^{L-1}-1} P(s_{j_0}|s_{i_0}) \\ \cdot\prod_{l=1}^{L-1} P(s_{j,l}|s_{i,l})\left\|(s_{i_0} - s_{j_0})\boldsymbol{\alpha}_0 + \sum_{l=1}^{L-1}(s_{i,l} - s_{j,l})\boldsymbol{\alpha}_l\right\|^2, \end{aligned}$$

which can further be expanded as

$$\begin{aligned} D_C = {} & \frac{1}{M^L}\sum_{i_0=0}^{M-1}\sum_{j_0=0}^{M-1} P(s_{j_0}|s_{i_0})(s_{i_0} - s_{j_0})^2\|\boldsymbol{\alpha}_0\|^2 \\ & \cdot\sum_{i=0}^{M^{L-1}-1}\sum_{j=0}^{M^{L-1}-1}\prod_{l=1}^{L-1} P(s_{j,l}|s_{i,l}) \\ & + \frac{2}{M^L}\sum_{i_0=0}^{M-1}\sum_{j_0=0}^{M-1} P(s_{j_0}|s_{i_0})(s_{i_0} - s_{j_0})\boldsymbol{\alpha}_0^{\top} \\ & \cdot\sum_{i=0}^{M^{L-1}-1}\sum_{j=0}^{M^{L-1}-1}\prod_{l=1}^{L-1} P(s_{j,l}|s_{i,l})\left(\sum_{l=1}^{L-1}(s_{i,l} - s_{j,l})\boldsymbol{\alpha}_l\right) \\ & + \frac{1}{M^L}\sum_{i=0}^{M^{L-1}-1}\sum_{j=0}^{M^{L-1}-1}\prod_{l=1}^{L-1} P(s_{j,l}|s_{i,l})\left\|\sum_{l=1}^{L-1}(s_{i,l} - s_{j,l})\boldsymbol{\alpha}_l\right\|^2 \\ & \cdot\sum_{i_0=0}^{M-1}\sum_{j_0=0}^{M-1} P(s_{j_0}|s_{i_0}). \end{aligned} \tag{61}$$

To investigate each of the three terms, let us analyze them individually. For the first term, we can define $\mathbf{s}_i' = [s_{i,1}, s_{i,2}, \ldots, s_{i,L-1}]^\top$ and rewrite the tail part as

$$\begin{aligned}
&\sum_{i=0}^{M^{L-1}-1}\sum_{j=0}^{M^{L-1}-1}\prod_{l=1}^{L-1}P\big(s_{j,l}|s_{i,l}\big)\\
&=\sum_{\mathbf{s}_i'\in\{0,1,\ldots,M-1\}^{L-1}}\sum_{\mathbf{s}_j'\in\{0,1,\ldots,M-1\}^{L-1}}\prod_{l=1}^{L-1}P\big(s_{j,l}|s_{i,l}\big)\\
&=\sum_{\mathbf{s}_i'\in\{0,1,\ldots,M-1\}^{L-1}}\sum_{\mathbf{s}_j'\in\{0,1,\ldots,M-1\}^{L-1}}P\Big(\mathbf{s}_j'|\mathbf{s}_i'\Big).
\end{aligned}$$

Note that $\mathbf{P}'$, with $P'(i,j) = P(\mathbf{s}_j'|\mathbf{s}_i')$, is a stochastic matrix with row sums equal to 1. Hence, the above expression equals to M^{L-1}. We can then rewrite the first term as

$$\frac{1}{M^L}\sum_{i_0=0}^{M-1}\sum_{j_0=0}^{M-1}P\big(s_{j_0}|s_{i_0}\big)\big(s_{i_0}-s_{j_0}\big)^2\|\boldsymbol{\alpha}_0\|^2\times M^{L-1}.$$

By substituting $s_{i_0} = i$, $s_{j_0} = j$, and $Q_M(i,j) = P(s_{j_0}|s_{i_0})$ into the above expression, we have

$$\frac{1}{M}\sum_{i_0=0}^{M-1}\sum_{j_0=0}^{M-1}Q_M(i,j)(i-j)^2\|\boldsymbol{\alpha}_0\|^2.$$

For the second term, since $\mathbf{Q}_M$ is symmetric, we have $P(s_{j_0}|s_{i_0}) = P(s_{i_0}|s_{j_0})$. Then the sum involving s_{i_0} and s_{j_0} can be rewritten as

$$\begin{aligned}
&\sum_{i_0=0}^{M-1}\sum_{j_0=0}^{M-1}P\big(s_{j_0}|s_{i_0}\big)\big(s_{i_0}-s_{j_0}\big)\boldsymbol{\alpha}_0^\top\\
&=\frac{1}{2}\sum_{i_0=0}^{M-1}\sum_{j_0=0}^{M-1}P\big(s_{j_0}|s_{i_0}\big)\big(s_{i_0}-s_{j_0}\big)\boldsymbol{\alpha}_0^\top\\
&\quad+\frac{1}{2}\sum_{i_0=0}^{M-1}\sum_{j_0=0}^{M-1}P\big(s_{i_0}|s_{j_0}\big)\big(s_{i_0}-s_{j_0}\big)\boldsymbol{\alpha}_0^\top\\
&=\frac{1}{2}\sum_{i_0=0}^{M-1}\sum_{j_0=0}^{M-1}P\big(s_{j_0}|s_{i_0}\big)\big(s_{i_0}-s_{j_0}\big)\boldsymbol{\alpha}_0^\top\\
&\quad+\frac{1}{2}\sum_{i_0=0}^{M-1}\sum_{j_0=0}^{M-1}P\big(s_{j_0}|s_{i_0}\big)\big(s_{j_0}-s_{i_0}\big)\boldsymbol{\alpha}_0^\top\\
&=\frac{1}{2}\sum_{i_0=0}^{M-1}\sum_{j_0=0}^{M-1}P\big(s_{j_0}|s_{i_0}\big)\big(\big(s_{i_0}-s_{j_0}\big)+\big(s_{j_0}-s_{i_0}\big)\big)\boldsymbol{\alpha}_0^\top\\
&=\mathbf{0}^\top.
\end{aligned}$$

Therefore, the second term in (61) is zero since it involves an inner product with a zero vector.

For the third term, similar to the first term, we have

$$\sum_{i_0=0}^{M-1}\sum_{j_0=0}^{M-1}P\big(s_{j_0}|s_{i_0}\big)=M,$$

and the third term can be expressed as

$$\frac{1}{M^{L-1}}\sum_{i=0}^{M^{L-1}-1}\sum_{j=0}^{M^{L-1}-1}\prod_{l=1}^{L-1}P\big(s_{j,l}|s_{i,l}\big)\Big\|\sum_{l=1}^{L-1}\big(s_{i,l}-s_{j,l}\big)\boldsymbol{\alpha}_l\Big\|^2.$$

Therefore, we can simplify (61) as

$$\begin{aligned}
D_C=&\frac{1}{M}\sum_{i=0}^{M-1}\sum_{j=0}^{M-1}Q_M(i,j)(i-j)^2\|\boldsymbol{\alpha}_0\|^2\\
&+\frac{1}{M^{L-1}}\sum_{i=0}^{M^{L-1}-1}\sum_{j=0}^{M^{L-1}-1}\prod_{l=1}^{L-1}P\big(s_{j,l}|s_{i,l}\big)\\
&\times\Big\|\sum_{l=1}^{L-1}\big(s_{i,l}-s_{j,l}\big)\boldsymbol{\alpha}_l\Big\|^2. \qquad (62)
\end{aligned}$$

The second term in the above equation can be interpreted as the channel MSD for $L-1$, and it can be decomposed using the same method as in (61). Hence, we can express (62) as

$$\begin{aligned}
D_C=&\frac{1}{M}\sum_{i=0}^{M-1}\sum_{j=0}^{M-1}Q_M(i,j)(i-j)^2\Big(\|\boldsymbol{\alpha}_0\|^2+\|\boldsymbol{\alpha}_1\|^2\Big)\\
&+\frac{1}{M^{L-2}}\sum_{i=0}^{M^{L-2}-1}\sum_{j=0}^{M^{L-2}-1}\prod_{l=2}^{L-1}P\big(s_{j,l}|s_{i,l}\big)\Big\|\sum_{l=2}^{L-1}\big(s_{i,l}-s_{j,l}\big)\boldsymbol{\alpha}_l\Big\|^2.
\end{aligned}$$

By repeating the same operation, we can obtain a recursive summation, which is shown as

$$D_C=\frac{1}{M}\sum_{i=0}^{M-1}\sum_{j=0}^{M-1}Q_M(i,j)(i-j)^2\sum_{l=0}^{L-1}\|\boldsymbol{\alpha}_l\|^2.$$

By applying the definition of E_M in (22), we can demonstrate that the above expression is equivalent to (21). Hence, we have established the proof for Proposition 2.

APPENDIX B
PROOF OF COROLLARY 3

Since $\mathbf{Q}_M$ is a doubly stochastic matrix, its largest eigenvalue is $\lambda_0 = 1$, and all other eigenvalues are smaller than 1. Let p_j denote $\hat{Q}_M(0,j)$. Based on the property of M-PSK as given in (39), the eigenvalues can be written as

$$\lambda_k=\sum_{j=0}^{M-1}\hat{Q}_M(0,j)\cos\Big(\frac{2\pi k}{M}(j-0)\Big)=\sum_{j=0}^{M-1}p_j\cos\Big(\frac{2\pi k}{M}j\Big).$$

In this proof, we only consider even values of M. The cases of odd M can be proven similarly. We define a vector $\mathbf{w}^{(k)} = [w_0^{(k)}, w_1^{(k)}, \ldots, w_{M/2}^{(k)}]^\top$ with

$$w_i^{(k)}=\begin{cases}\frac{1}{2}\cos\Big(\frac{2ik\pi}{M}\Big), & i=0,\frac{M}{2},\\ \cos\Big(\frac{2ik\pi}{M}\Big), & i=1,2,\ldots,\frac{M}{2}-1.\end{cases}$$

Since $p_j = p_{M-j}$ holds for the channel matrix of M-PSK, we can rewrite λ_k as

$$\lambda_k=2\sum_{j=0}^{\frac{M}{2}}p_jw_j^{(k)},$$

which can further be expanded as

$$\lambda_k = 2\Bigg(p_{\frac{M}{2}} \sum_{j=0}^{\frac{M}{2}} w_j^{(k)} + \left(p_{\frac{M}{2}-1} - p_{\frac{M}{2}}\right) \sum_{j=0}^{\frac{M}{2}-1} w_j^{(k)} + \cdots + (p_0 - p_1) w_0^{(k)}\Bigg). \tag{63}$$

It is worth noting that, for $i = 1, 2, \ldots, M/2$, the inequality $p_{i-1} - p_i \geq 0$ holds due to the property given in (39). According to [50], a sufficient condition for $\lambda_1 \geq \lambda_k$ is

$$\sum_{j=0}^{l} w_j^{(k)} \leq \sum_{j=0}^{l} w_j^{(1)}, \quad l = 0, \ldots, \frac{M}{2}, \ k = 2, \ldots, M-2. \tag{64}$$

Note that $k = M-1$ is not involved since $\lambda_1 = \lambda_{M-1}$. We will prove the sufficient condition in (64). For $l = \frac{M}{2}$, the left-hand side term in (64) is a constant, given by

$$\sum_{j=0}^{\frac{M}{2}} w_j^{(k)} = \sum_{j=0}^{M-1} \frac{1}{2} \cos\left(\frac{2\pi k}{M} j\right) = 0. \tag{65}$$

Note that the values are independent of k. Hence, the equality in (64) holds for $l = \frac{M}{2}$.

For other values of l, the left-hand-side terms in (64) can be rewritten as

$$\begin{aligned}\sum_{j=0}^{l} w_j^{(k)} &= \frac{1}{2} \sum_{j=-l}^{l} \exp\left(\frac{i2\pi k}{M} j\right) \\ &= \frac{1}{2} \frac{1 - \left(\exp\left(\frac{i2\pi k}{M}\right)\right)^{2l+1}}{\left(\exp\left(\frac{i2\pi k}{M}\right)\right)^{l} \left(1 - \left(\exp\left(\frac{i2\pi k}{M}\right)\right)\right)}.\end{aligned}$$

By applying Euler's formula, double-angle identities, and sum-to-product identities (c.f. Appendix C (6)), we can simplify the above expression as

$$\sum_{j=0}^{l} w_j^{(k)} = \frac{1}{2} \frac{\sin\left((2l+1)\frac{\pi k}{M}\right)}{\sin\left(\frac{\pi k}{M}\right)}. \tag{66}$$

Let us define $a_{2l+1}(k) \triangleq \frac{\sin((2l+1)\frac{\pi k}{M})}{\sin(\frac{\pi k}{M})}$. To prove (64), we need to show that $a_{2l+1}(1) \geq a_{2l+1}(k)$ for all l. Since $a_{2l+1}(1)$ is always positive, a sufficient condition for $a_{2l+1}(1) \geq a_{2l+1}(k)$ is that $a_{2l+1}^2(1) \geq a_{2l+1}^2(k)$. By introducing the ratio between $a_{2l+1}^2(k)$ and $a_{2l+1}^2(1)$, we have

$$\left(\frac{a_{2l+1}(k)}{a_{2l+1}(1)}\right)^2 = \frac{\left(\frac{\sin\left((2l+1)\frac{\pi k}{M}\right)}{\sin\left(\frac{\pi k}{M}\right)}\right)^2}{\left(\frac{\sin\left((2l+1)\frac{\pi}{M}\right)}{\sin\left(\frac{\pi}{M}\right)}\right)^2} = \frac{\frac{1}{k}\left(\frac{\sin\left((2l+1)\frac{\pi k}{M}\right)}{\sin\left((2l+1)\frac{\pi}{M}\right)}\right)^2}{\frac{1}{k}\left(\frac{\sin\left(\frac{\pi k}{M}\right)}{\sin\left(\frac{\pi}{M}\right)}\right)^2}, \tag{67}$$

for $l = 1, 2, \ldots, \frac{M}{2} - 1$, $k = 2, 3, \ldots, \frac{M}{2}$. We aim to prove that (67) is always smaller than 1, which is a sufficient condition for $a_{2l+1}(1) \geq a_{2l+1}(k)$. Note that we only consider half of the range of k since we have $a_{2l+1}(k) = a_{2l+1}(M-k)$. To do this, we introduce the definition of *Fejèr kernel* [51].

Definition 2: The Fejèr kernel is a closed-form expression given by

$$F_n(x) = \frac{1}{n}\left(\frac{\sin\left(\frac{nx}{2}\right)}{\sin\left(\frac{x}{2}\right)}\right)^2, \tag{68}$$

where $n \in \mathbb{Z}^+$ and $x \in \mathbb{R}$.

Relax l to a continuous variable $l \in [0, \frac{M}{2} - 1]$, and define $x = \frac{2\pi(2l+1)}{M}$. The ratio in (67) can be expressed as a ratio of two Féjer kernels, i.e.,

$$\left(\frac{a_{2l+1}(k)}{a_{2l+1}(1)}\right)^2 = \frac{F_k(x)}{F_k\left(\frac{2\pi}{M}\right)}, \quad \frac{2\pi}{M} \leq x \leq \pi, \ k = 2, 3, \ldots, \frac{M}{2}. \tag{69}$$

Note that here we also only consider half of the range of x since $F_k(x) = F_k(2\pi - x)$.

To prove that (69) is smaller than 1, we divide the range of x into two parts, based on the first root of the Féjer kernel. To obtain roots of $F_k(x)$, we set $F_k(x_n) = 0$ and then obtain

$$x_n = \frac{2n\pi}{k}, \quad n = 1, 2, \ldots, \left\lfloor \frac{k}{2} \right\rfloor. \tag{70}$$

Note that $x_1 = \frac{2\pi}{k}$. Since $F_k(x)$ is monotonically decreasing for $x \in [0, \frac{2\pi}{k}]$, we can prove that $F_k(x) \leq F_k(\frac{2\pi}{M})$ for $\frac{2\pi}{M} \leq x < x_1$, i.e.,

$$F_k\left(\frac{2\pi}{M}\right) > F_k(x), \quad \frac{2\pi}{M} < x \leq \frac{2\pi}{k}, \quad k = 2, 3, \ldots, \frac{M}{2}. \tag{71}$$

For $x_1 \leq x \leq \pi$, we derive an upper bound on $F_k(x)$ as

$$\begin{aligned}F_k(x) &= \frac{1}{k}\left(\frac{\sin\left(\frac{kx}{2}\right)}{\sin\left(\frac{x}{2}\right)}\right)^2 \leq \frac{1}{k}\left(\frac{\sin\left(\frac{kx}{2}\right)}{\frac{x}{\pi}}\right)^2 \\ &= \frac{\pi^2 k}{4}\left(\frac{\sin\left(\frac{kx}{2}\right)}{\frac{kx}{2}}\right)^2 \overset{(d)}{\leq} \frac{\pi^2 k}{4} \cdot \frac{4}{9\pi^2} = \frac{k}{9},\end{aligned} \tag{72}$$

where (d) follows from the fact that the absolute value of a sinc function in the domain $[\pi, \frac{k\pi}{2}]$ is upper bounded by $|\mathrm{sinc}(\frac{3\pi}{2})|$. Besides, we derive a lower bound on $F_k(\frac{2\pi}{M})$ as

$$\begin{aligned}F_k\left(\frac{2\pi}{M}\right) &= \frac{1}{k}\left(\frac{\sin\left(\frac{\pi k}{M}\right)}{\sin\left(\frac{\pi}{M}\right)}\right)^2 > k\left(\frac{\sin\left(\frac{\pi k}{M}\right)}{\frac{\pi k}{M}}\right)^2 \\ &\overset{(e)}{\geq} k\left(\frac{\sin\left(\frac{\pi}{2}\right)}{\frac{\pi}{2}}\right)^2 = \frac{4k}{\pi^2},\end{aligned} \tag{73}$$

where (e) follows from the fact that a sinc function is decreasing in the domain $[\frac{2\pi}{M}, \frac{\pi}{2}]$. It can be observed

from (72) and (73) that the lower bound on $F_k(\frac{2\pi}{M})$ is greater than the upper bound on $F_k(x)$. Sufficiently, we deduce that

$$F_k\left(\frac{2\pi}{M}\right) > F_k(x), \quad \frac{2\pi}{k} \le x \le \pi, \ k = 2, 3, \ldots, \frac{M}{2}. \tag{74}$$

By combining (71) and (74), we obtain

$$F_k\left(\frac{2\pi}{M}\right) > F_k(x), \ \frac{2\pi}{M} < x < 2\pi - \frac{2\pi}{M}, \ k = 2, \ldots, \frac{M}{2}. \tag{75}$$

Since $x = \frac{2\pi(2l+1)}{M}$, we obtain that (75) holds for $l \in [0, \frac{M}{2} - 1]$. Since the range of l in (67) is a subset of $l \in [0, \frac{M}{2} - 1]$, the inequality (75) serves as a sufficient condition to establish that the ratio stated in (67) is always less than 1. Therefore, we have demonstrated (64) as a sufficient condition for Corollary 3.

APPENDIX C
MATHEMATICAL TOOLS AND FORMULAS

In this Appendix, we provide a collection of formulas and properties from several mathematical fields, including linear algebra, that serve as fundamental mathematical tools used in this paper.

(1) Lexicographic order for integer vectors: Suppose two integer vectors $\mathbf{x}, \mathbf{y} \in \mathbb{Z}^n$ and $\mathbf{x} \neq \mathbf{y}$. The vector $\mathbf{x}$ is smaller than $\mathbf{x}$ in lexicographic order, denoted as

$$\mathbf{x} <_{\text{lex}} \mathbf{y},$$

if and only if the first coordinate where $\mathbf{x}$ and $\mathbf{y}$ differ, say x_i and y_i, respectively, satisfies $x_i < y_i$.

(2) For column vectors $\mathbf{x}, \mathbf{y} \in \mathbb{R}^n$, $\text{Tr}(\mathbf{x}\mathbf{y}^\top) = \mathbf{y}^\top\mathbf{x}$.

(3) For column vectors $\mathbf{x}_i \in \mathbb{R}^n$, $i = 0, 1, \ldots, L-1$, the multinomial theorem is

$$\left\| \sum_{i=0}^{L-1} \mathbf{x}_i \right\|^2 = \sum_{i=0}^{L-1} \sum_{i=0}^{L-1} \mathbf{x}_i^\top \mathbf{x}_j.$$

(4) Sum of squares formula:

$$1^2 + 2^2 + \cdots + n^2 = \frac{n(n+1)(2n+1)}{6}.$$

(5) Eigenpair of the Kronecker product: Suppose that $(\lambda, \mathbf{u})$ and $(\omega, \mathbf{v})$ are eigenpairs of matrices $\mathbf{A}$ and $\mathbf{B}$, respectively, then $(\lambda\omega, \mathbf{u} \otimes \mathbf{v})$ is an eigenpair of the Kronecker product matrix $\mathbf{A} \otimes \mathbf{B}$.

(6) Some formulas for trigonometric functions:
Euler's formula:

$$e^{i\alpha} = \cos(\alpha) + i\sin(\alpha).$$

Double-angle identities:

$$\begin{cases} \cos(2\alpha) = 1 - 2\sin^2(\alpha), \\ \sin(2\alpha) = 2\sin(\alpha)\cos(\alpha). \end{cases}$$

Sum-to-product identities:

$$\begin{cases} \cos(\alpha) - \cos(\beta) = -2\sin\left(\frac{\alpha+\beta}{2}\right)\sin\left(\frac{\alpha-\beta}{2}\right), \\ \sin(\alpha) - \sin(\beta) = 2\cos\left(\frac{\alpha+\beta}{2}\right)\sin\left(\frac{\alpha-\beta}{2}\right). \end{cases}$$

REFERENCES

[1] Y. Yao and W. H. Mow, "Near-optimal nonbinary index assignment for equiprobable uniform quantizers and M-PSK transmission," in *Proc. IEEE Int. Conf. Commun.*, Dublin, Ireland, 2020, pp. 1–6.

[2] P. Gandotra, R. K. Jha, and S. Jain, "Green communication in next generation cellular networks: A survey," *IEEE Access*, vol. 5, pp. 11727–11758, 2017.

[3] O. Elijah, T. A. Rahman, I. Orikumhi, C. Y. Leow, and M. H. D. N. Hindia, "An overview of Internet of Things (IoT) and data analytics in agriculture: Benefits and challenges," *IEEE Internet Things J.*, vol. 5, no. 5, pp. 3758–3773, Oct. 2018.

[4] I. Khan, F. Belqasmi, R. Glitho, N. Crespi, M. Morrow, and P. Polakos, "Wireless sensor network virtualization: A survey," *IEEE Commun. Surveys Tuts.*, vol. 18, no. 1, pp. 553–576, 1st Quart., 2016.

[5] J. M. Williams et al., "Weaving the wireless Web: Toward a low-power, dense wireless sensor network for the Industrial IoT," *IEEE Microw. Mag.*, vol. 18, no. 7, pp. 40–63, Nov./Dec. 2017.

[6] T. Wimalajeewa and P. K. Varshney, "Application of compressive sensing techniques in distributed sensor networks: A survey," 2017, *arXiv:1709.10401*.

[7] I. F. Akyildiz and M. C. Vuran, *Wireless Sensor Networks*, vol. 4. Hoboken, NJ, USA: Wiley, 2010,

[8] S. Karimi-Bidhendi, J. Guo, and H. Jafarkhani, "Energy-efficient node deployment in heterogeneous two-tier wireless sensor networks with limited communication range," *IEEE Trans. Wireless Commun.*, vol. 20, no. 1, pp. 40–55, Jan. 2021.

[9] A. Shirazinia, S. Chatterjee, and M. Skoglund, "Joint source-channel vector quantization for compressed sensing," *IEEE Trans. Signal Process.*, vol. 62, no. 14, pp. 3667–3681, Jul. 2014.

[10] X. Yu, H. Wang, and E. Yang, "Design and analysis of optimal noisy channel quantization with random index assignment," *IEEE Trans. Inf. Theory*, vol. 56, no. 11, pp. 5796–5804, Nov. 2010.

[11] S. Dumitrescu, "On the design of optimal noisy channel scalar quantizer with random index assignment," *IEEE Trans. Inf. Theory*, vol. 62, no. 2, pp. 724–735, Feb. 2016.

[12] Y. M. Saidutta, A. Abdi, and F. Fekri, "Joint source-channel coding over additive noise analog channels using mixture of variational autoencoders," *IEEE J. Sel. Areas Commun.*, vol. 39, no. 7, pp. 2000–2013, Jul. 2021.

[13] R. Hagen and P. Hedelin, "Robust vector quantization by a linear mapping of a block code," *IEEE Trans. Inf. Theory*, vol. 45, no. 1, pp. 200–218, Jan. 1999.

[14] X. Wang and X. Wu, "Index assignment optimization for joint source-channel MAP decoding," in *Proc. IEEE Inf. Theory Workshop*, 2006, pp. 308–312.

[15] M. Leinonen, M. Codreanu, and M. Juntti, "Channel-robust compressed sensing via vector pre-quantization in wireless sensor networks," in *Proc. IEEE Global Conf. Signal Inf. Process*, Orlando, FL, USA, Dec. 2015, pp. 383–387.

[16] M. Skoglund, "On channel-constrained vector quantization and index assignment for discrete memoryless channels," *IEEE Trans. Inf. Theory*, vol. 45, no. 7, pp. 2615–2622, Nov. 1999.

[17] Y. Yamaguchi and T. Huang, "Optimum binary fixed-length block codes," MIT Res. Lab. Electron., Cambridge, MA, USA, Rep. 78, 1965.

[18] T. Huang et al., "Optimum binary code," MIT Res. Lab. Electron., Cambridge, MA, USA, Rep. 82, 1966.

[19] T. Crimmins, H. Horwitz, C. Palermo, and R. Palermo, "Minimization of mean-square error for data transmitted via group codes," *IEEE Trans. Inf. Theory*, vol. IT-15, no. 1, pp. 72–78, Jan. 1969.

[20] S. W. McLaughlin, D. L. Neuhoff, and J. J. Ashley, "Optimal binary index assignments for a class of equiprobable scalar and vector quantizers," *IEEE Trans. Inf. Theory*, vol. 41, no. 6, pp. 2031–2037, Nov. 1995.

[21] B. Farber and K. Zeger, "Quantizers with uniform encoders and channel optimized decoders," *IEEE Trans. Inf. Theory*, vol. 50, no. 1, pp. 62–77, Jan. 2004.

[22] E. M. Loiola, N. M. M. de Abreu, P. O. Boaventura-Netto, P. Hahn, and T. Querido, "A survey for the quadratic assignment problem," *Eur. J. Oper. Res.*, vol. 176, no. 2, pp. 657–690, Jan. 2007.

[23] K. Zeger and A. Gersho, "Pseudo-Gray coding," *IEEE Trans. Commun.*, vol. 38, no. 12, pp. 2147–2158, Dec. 1990.

[24] N. Farvardin, "A study of vector quantization for noisy channels," *IEEE Trans. Inf. Theory*, vol. 36, no. 4, pp. 799–809, Jul. 1990.

[25] P. Knagenhjelm and E. Agrell, "The Hadamard transform—A tool for index assignment," *IEEE Trans. Inf. Theory*, vol. 42, no. 4, pp. 1139–1151, Jul. 1996.
[26] J.-K. Han and H.-M. Kim, "Classified VQ codebook index assignment for communication over noisy channels," *IEEE Trans. Circuits Syst. Video Technol.*, vol. 9, no. 3, pp. 451–458, Apr. 1999.
[27] S. Gadkari and K. Rose, "Robust vector quantizer design by noisy channel relaxation," *IEEE Trans. Commun.*, vol. 47, no. 8, pp. 1113–1116, Aug. 1999.
[28] X. Wang and X. Wu, "Index assignment optimization for joint source-channel MAP decoding," *IEEE Trans. Commun.*, vol. 58, no. 3, pp. 901–910, Mar. 2010.
[29] H. Skinnemoen, "Modulation organized vector quantization, MOR-VQ," in *Proc. IEEE Int. Symp. Inf. Theory*, Trondheim, Norway, 1994, p. 238.
[30] D. Qiao, W. H. Mow, and C. Leung, "Scalar quantizers with uniform encoders and channel-optimized decoders for M-PSK schemes," in *Proc. IEEE GLOBECOM*, Miami, FL, USA, Dec. 2010, pp. 1–5.
[31] G. Ben-David and D. Malah, "Bounds on the performance of vector-quantizers under channel errors," *IEEE Trans. Inf. Theory*, vol. 51, no. 6, pp. 2227–2235, Jun. 2005.
[32] X. Wu, H. D. Mittelmann, X. Wang, and J. Wang, "On computation of performance bounds of optimal index assignment," *IEEE Trans. Commun.*, vol. 59, no. 12, pp. 3229–3233, Dec. 2011.
[33] H. Chan, W. H. Mow, and C. Leung, "Index assignment for scalar quantization with M-ary phase shift keying," in *Proc. IEEE Int. Symp. Inf. Theory*, Adelaide, SA, USA, Sep. 2005, pp. 357–361.
[34] Y. Yao and W. H. Mow, "Optimal index assignment for scalar quantizers and M-PSK via a discrete convolution-rearrangement inequality," in *Proc. IEEE Int. Symp. Inf. Theory*, 2021, pp. 1153–1158.
[35] R. M. Gray and D. L. Neuhoff, "Quantization," *IEEE Trans. Inf. Theory*, vol. 44, no. 6, pp. 2325–2383, Oct. 1998.
[36] A. Vasuki and P. T. Vanathi, "A review of vector quantization techniques," *IEEE Potentials*, vol. 25, no. 4, pp. 39–47, Jul./Aug. 2006.
[37] A. Mehes and K. Zeger, "Binary lattice vector quantization with linear block codes and affine index assignments," *IEEE Trans. Inf. Theory*, vol. 44, no. 1, pp. 79–94, Jan. 1998.
[38] W.-Y. Chan, S. Gupta, and A. Gersho, "Enhanced multistage vector quantization by joint codebook design," *IEEE Trans. Commun.*, vol. 40, no. 11, pp. 1693–1697, Nov. 1992.
[39] W.-W. Chang, T.-H. Tan, and D.-Y. Wang, "Robust vector quantization for wireless channels," *IEEE J. Sel. Areas Commun.*, vol. 19, no. 7, pp. 1365–1373, Jul. 2001.
[40] A. Mehes and K. Zeger, "Randomly chosen index assignments are asymptotically bad for uniform sources," *IEEE Trans. Inf. Theory*, vol. 45, no. 2, pp. 788–794, Mar. 1999.
[41] D. Messerschmitt, "Quantizing for maximum output entropy (corresp.)," *IEEE Trans. Inf. Theory*, vol. IT-17, no. 5, pp. 612–612, Sep. 1971.
[42] N. Farvardin and V. Vaishampayan, "On the performance and complexity of channel-optimized vector quantizers," *IEEE Trans. Inf. Theory*, vol. 37, no. 1, pp. 155–160, 1991.
[43] J.-B. Hiriart-Urruty and J. Malick, "A fresh variational-analysis look at the positive semidefinite matrices world," *J. Optim. Theory. Appl.*, vol. 153, no. 3, pp. 551–577, Jan. 2012.
[44] J. G. Proakis and M. Salehi, *Digital Communications*. New York, NY, USA: McGraw-Hill, 2001.
[45] M.-M. Deza and E. Deza, *Dictionary of Distances*. Amsterdam, The Netherlands: Elsevier, 2006.
[46] S. Cui, A. J. Goldsmith, and A. Bahai, "Energy-constrained modulation optimization," *IEEE Trans. Wireless Commun.*, vol. 4, no. 5, pp. 2349–2360, Sep. 2005.
[47] F. M. Costa and H. Ochiai, "A comparison of modulations for energy optimization in wireless sensor network links," in *Proc. IEEE GLOBECOM*, Miami, FL, USA, 2010, pp. 1–5.
[48] F. M. Costa and H. Ochiai, "Energy-efficient physical layer design for wireless sensor network links," in *Proc. IEEE Int. Conf. Commun.*, Kyoto, Japan, 2011, pp. 1–5.
[49] S. Chouhan, R. Bose, and M. Balakrishnan, "A framework for energy-consumption-based design space exploration for wireless sensor nodes," *IEEE Trans. Comput.-Aided Design Integr. Circuits Syst.*, vol. 28, no. 7, pp. 1017–1024, Jul. 2009.
[50] B. Simon, *Convexity: An Analytic Viewpoint*. Cambridge, U.K.: Cambridge Univ. Press, 2011.
[51] K. Hoffman, *Banach Spaces of Analytic Functions*. Englewood Cliffs, NJ, USA: Prentice-Hall, 1962.

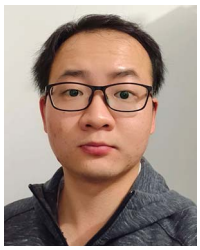

YUNXIANG YAO (Student Member, IEEE) received the B.Eng. degree in optoelectronic engineering and optical communication from the University of Electronic Science and Technology of China, Chengdu, China, in 2016. He is currently pursuing the Ph.D. degree in electronic and computer engineering with The Hong Kong University of Science and Technology, Hong Kong, China. His research interests include communication theory, joint source-channel coding, and low-power bus coding.

WAI HO MOW (Senior Member, IEEE) received the Ph.D. degree in information engineering from the Chinese University of Hong Kong in 1993. From 1997 to 1999, he was with the Nanyang Technological University, Singapore. He has been with the Hong Kong University of Science and Technology since 2000 and is currently a Professor. He unified all known constructions of perfect roots-of-unity (aka CAZAC) sequences, which have been widely used as communication preambles and radar signals. He published two books and 220+ journal/conference publications and is the inventor of 38 patents. He pioneered the lattice approach to signal detection problems, including sphere decoding and complex lattice reduction-aided detection. His research areas include coding and information theory, wireless communications, optical camera communications, and thermographic signal processing. His joint work won the top prizes of 10+ project/paper competitions, including the 2014 HK U-21 IoT Gold Award for Revolutional Concept, the Best Paper Award of 2013 and 2016 Asia–Pacific Communications Conference, and the Best Mobile App Award at ACM MobiCom'2013. His co-invented picture barcode PiCode was highlighted as one of the four local innovations in the 2015 International IT Fest organized by the Office of the Government Chief Information Officer, Hong Kong. He served on the editorial boards of six journals, including the IEEE TRANSACTIONS ON WIRELESS COMMUNICATIONS. He is a Past Chair of the Hong Kong Chapter of the IEEE Information Theory Society, and was the general/program chair of six conferences, incl. SETA'2018 held in Hong Kong. He is a Past Member of the Radio Spectrum Advisory Committee, Office of the Telecommunications Authority of the Hong Kong S.A.R. Government.